

2019-01-01

Non Linear Optics For Materials Fabrication And Medical Instrumentation

Aurelio Paez
University of Texas at El Paso

Follow this and additional works at: https://digitalcommons.utep.edu/open_etd



Part of the [Biophysics Commons](#), and the [Optics Commons](#)

Recommended Citation

Paez, Aurelio, "Non Linear Optics For Materials Fabrication And Medical Instrumentation" (2019). *Open Access Theses & Dissertations*. 2885.

https://digitalcommons.utep.edu/open_etd/2885

This is brought to you for free and open access by ScholarWorks@UTEP. It has been accepted for inclusion in Open Access Theses & Dissertations by an authorized administrator of ScholarWorks@UTEP. For more information, please contact lweber@utep.edu.

NON LINEAR OPTICS FOR MATERIALS FABRICATION AND
MEDICAL INSTRUMENTATION

AURELIO PAEZ

Doctoral Program in Materials Science and Engineering

APPROVED:

Chunqiang Li, Ph.D., Chair

David Roberson, Ph.D.

Katja Michael, Ph.D.

Stephen L. Crites, Jr., Ph.D.
Dean of the Graduate School

Copyright ©

by

Aurelio Paez

2019

Dedication

The sacrifices made by myself and so many around me for me to achieve my dreams of a PhD and subsequent employment at NASA cannot be understated, nor can they fit on a single page. First to my children, that made the ultimate sacrifice of time with their father. Aurora, whose never ending supply of puns, hugs and reminders got me through so many days. Natalie, a natural leader to her sisters, she helped me to keep order within the chaos and disorder. Michelle's personal drive for academic excellence inspired me to always be and do better. And Sarai, my little agent of chaos, where we all worked to reduce chaos, you added your own personal boisterous energies that juxtaposed beautifully with the seriousness of our lives. To you four I say, "we did it kiddos". Second, to my dad and brother, that were always there to support me emotionally and financially, I could not have done it without you. Third, to my mom, whom lost her battle with cancer at the very end of my studies, at least you got to introduce me to the oncologist as, "...my son the doctor...", I'm glad you got to see it, have peace momma. And finally, to Sierra, that helped me in every which way possible to give me the time and energy to have a fighting chance at finishing this endeavor, thank you, you stepped in when everything was falling apart and helped me to hold it all together, I am forever grateful.

NON LINEAR OPTICS FOR MATERIALS FABRICATION AND
MEDICAL INSTRUMENTATION

by

AURELIO PAEZ B.S. M.S

DISSERTATION

Presented to the Faculty of the Graduate School of

The University of Texas at El Paso

in Partial Fulfillment

of the Requirements

for the Degree of

DOCTOR OF PHILOSOPHY

MATERIALS SCIENCE AND ENGINEERING

THE UNIVERSITY OF TEXAS AT EL PASO

December 2019

Acknowledgements

I would like to acknowledge the guidance and patience given to me by my committee throughout my pursuit of the PhD. Their consistent support helped in ways I cannot put into words.

On the photo-cleavable material project, Dr. Katja Michael, Dr. Alfredo Ornelas, Phillip Baily, and Hector del Castillo worked on developing and creating the various iterations of the nitroindoline molecule that were fundamental to the project.

Roberto Iturralde and Mathew Weaver helped with the photo-cleaving project, learning quickly and taking the initiative to take the reins of the project in preparation for my departure.

Gilbert Navarro worked with me on the flow cytometer project, working long nights, and sometimes overnight and into the morning hours, with data collection and data processing. Gilbert took the initiative to learn the system in order to take over the project upon my departure.

Dr. Jianjun Sun, and Dr. Yanqing Bao produced the tagged cells that were used in the flow cytometer experiment. Culturing different cell types and offering input on the fluorescent characteristics of the samples.

Dr. David Roberson was always available for a quiet conversation and guidance on my projects and personal life.

Karla Carmona helped with formatting and proof reading of the final dissertation and constantly helped with finding funding opportunities throughout my academic career. Karla's help cannot be understated.

Dr. Chunqiang Li accepted me as a MASE PhD student in Fall of 2015 into his photonics lab in the physics department. In the time since, he has offered advice, guidance, critique, praise, admonishment, patience, support, motivation, laughter, an ear to listen, and quiet conversation. He

allowed me to pursue things how I wanted, interjecting when a course correction was in order. He was more than my advisor, he is my friend.

Abstract

Two-photon absorption is a nonlinear optical process where two photons are absorbed by a molecule simultaneously. The probability of this quantum phenomenon is proportional to the quadratic excitation of light intensity. It has many applications in biomedical and materials research, such as two-photon fluorescence microscopy. The first project is to apply two-photon absorption induced bond cleavage in photoreactive materials for engineering 3D tissue scaffolds. The major challenge for growing thick 3D tissues is the lack of vasculature, where nutrients and oxygen can be delivered to the growing cells. Our collaborators have synthesized a novel polypeptide that is composed of 34-mer chains of 5 hexapeptides linked covalently via 4 N-peptidyl-7-nitroindoline moieties. Femtosecond laser pulses are used to break the bonds in these nitroindoline moieties via two-photon absorption. Thus, disintegrating the structure of this polypeptide. Our long-term goal is to develop a novel hydrogel based on this photoreactive polypeptide and use two-photon absorption to fabricate tunnels mimicking vasculature. The second project is to develop an in vivo two-photon flow cytometer based on Airy beams. In vivo flow cytometry is a biomedical technique that can detect circulating cells in vivo. This early diagnosis technique is crucial for early cancer detections and immunological studies. The major challenge for such an optical instrument is the shallow penetration depth due to tissue scattering. Two-photon excitation utilizes near infrared wavelength lasers, which has deeper penetrations than one-photon excitation. Further we implemented non-diffracting laser beams, such as Airy beams, as the excitation source. These non-diffracting beams have long non-diffracting range (Rayleigh range) and the unique property of self-healing, i.e. recovering its spatial profile after tissue scattering. Therefore, non-diffracting beams can significantly increase the penetrations depth of light and make flow cytometry feasible for future clinical use.

Table of Contents

Dedication.....	iii
Acknowledgements.....	v
Abstract.....	vii
Table of Contents.....	viii
List of Figures.....	x
Chapter 1: Non-Linear Optics, 2-Photon Absorption Fluorescence.....	1
Non-Linear Optics.....	1
1-Photon Fluorescence.....	2
2-Photon Fluorescence.....	4
Photon Confinement.....	6
Mai-Tai.....	7
1-Photon Vs. 2-Photon.....	9
Chapter 2: 2-Photon for Tissue Engineering.....	11
Photo Cleavable Materials Project.....	11
Tissue Engineering.....	11
Prevasculariazation.....	12
Photo-Reactive Collagen-Like Peptides.....	13
2-Photon Microscope.....	14
Decay.....	14
UTEP Logo Mask.....	16
Peptide Hydrogel Photo-Cleaving, A Typical Case.....	20
Peptide Hydrogel: Area Of Interest.....	22
Peptide Hydrogel: 60 Minute Illumination.....	24
Non-Linear Optics Of New Materials.....	26
Results.....	28
Chapter 3 Flow Cytometer Using Non-Diffracting Light Beams.....	31
Flow Cytometry.....	31
Project Description & Unique Problems.....	31

Airy Beam.....	36
Optical Fourier Transform.....	37
Spatial Light Modulator (SLM).....	38
Optical Setup.....	39
In House Programs.....	40
Phase Masks.....	42
Z-Location of, and Co-Locating the Microchannel and Airy Sheet.....	45
Detection and Data Capture of Fluorescence Signal.....	48
Optimizations of the Flow Cytometer.....	52
Results.....	55
References.....	60
Appendix A: Python Code for Peak Finding.....	62
Appendix B: Python Code for Airy Mask Production.....	65
Appendix C: Python Code for Data Capture.....	68
Vita.....	70

List of Figures

Figure 1: Modified Jablonski Diagram	4
Figure 2: Two Photon Fluorescence Jablonski Diagram	5
Figure 3: Temporal Photon Confinement	7
Figure 4: Single VS Two Photon	9
Figure 5: Peptide Sequence	13
Figure 6: Raster Light Sheet Production	16
Figure 7: Demonstration of where the intermediate image plane is.	17
Figure 8: UTEP LogoMask	18
Figure 9: UTEP Logo at Different Exposition Times	19
Figure 10: Fluorescence Decay Examples	20
Figure 11: Tree Mask & Exposition	21
Figure 12: Pinstripe Mask	22
Figure 13: Focal Light Sheet Diagram	23
Figure 14: White light image of HydroGel, post 2-photon illumination.	24
Figure 15: Mask Removal Fluorescing	25
Figure 16: Post Illumination Sample	26
Figure 17: Molecule Decay Curves for 150 mW	29
Figure 18: Cross-section Diagram	32
Figure 19: Types of Beams	34
Figure 20: Bessel Beam	35
Figure 21: Airy Beam	36
Figure 22: 2-D Airy Beam	37
Figure 23: Optical setup of the Airy Beam Flow Cytometer	39
Figure 24: Example of the Airy Mask	42
Figure 25: Intensity of the Airy Beams Plot	46
Figure 26: Test and Diagnostics PMT300-1200hz-25mWGauss-single bead-1sec	51
Figure 27: Trace showing DAQ noise drop by isolating the PMT. At 2000000 samples the PMT was removed from the Optics table and placed on an electrical insulator.	53
Figure 28: Data without and with Dry ice	54
Figure 29: Results.	56
Figure 30: Fluoresce Tagging in a Biological Sample	58

Chapter 1: Non-Linear Optics, 2-photon absorption fluorescence

NON-LINEAR OPTICS

We begin by expressing the polarization of a material, wherein the polarization is proportional to the electric field E .

$$P(t) = \epsilon_0 \chi E \tag{1}$$

P is the polarization, χ is the susceptibility, and the permittivity of space is ϵ_0 . In this case as the E field increases so does the polarization. Increasing the E field until it begins to approach the energy of the electric field between atoms, signals a change in the polarizability- E field relationship. The reaction is now weakly linear because of slight changes in the material itself, leading to changes in the polarization. In order to describe this energy and polarization change we take a Taylor expansion of the polarization equation in E ,

$$P(t) = \epsilon_0 (\chi^1 E(t) + \chi^2 E^2(t) + \chi^3 E^3(t) + \dots) \tag{2}$$

P continues to be polarization, and E is the electric field. χ is the material's susceptibility, represented as a tensor that includes information about the material's crystal symmetry and polarizability. The material response is changing as the intensity of the light increases. The first order term is what we consider linear optics, and the higher order terms hold non-linear optical phenomena. As an example χ^1 corresponds to properties such as index of refraction, and absorption. χ^2 corresponds to second-harmonic generation and other parametric effects. Raman and Brillouin scattering, third-harmonic generation and 2-photon fluorescence belong to the χ^3 term class of material responses. (Rulliere 2005)

2-photon fluorescence was predicted in 1931 by Maria Goeppert Mayer, when she submitted her 13-page dissertation “Elementary processes with two quantum transitions” wherein she describes the probability of 2-photon absorption and writes about non-linear material responses (Goeppert-Mayer, Maria; Göttinger 1931). The dissertation states that, given that a bound electron can absorb a photon of energy E , then there is a possibility that 2 photons, whose energy sum to E , could be absorbed. We will cover this in more detail later. It would take 30 years, and the invention of the light-amplification-by-stimulated-emission-of-radiation device (laser) before she was proved correct by Kaiser and Garret in 1961 (Kaiser 1961). In their paper they showed that 1-photon fluorescence and 2-photon fluorescence could be achieved for a solution of $\text{CaF}_2\text{Eu}^{2+}$. Let us describe first the 1-photon, then the 2-photon case of fluorescence.

1-PHOTON FLUORESCENCE

1-photon fluorescence occurs when an electron can absorb energy from impinging photons of some energy, where the photon energy E is given by,

$$E_{\text{photon}} = \frac{hc}{\lambda} = h\nu \quad 3$$

where h is Planck’s constant, c is the speed of light, λ is the wavelength of the photon, and ν is the photon frequency, and subsequently emit photons of some energy less than the original photon energy.

Assume that a system’s electron is at some ground state S_0 , and that it can absorb an incoming photon, absorbing a photon gives the system some energy, $h\nu$. The energy is then,

4

$$S_0 + E_{excite}$$

and is considered excitation of the system to some new state S_1 . The photon responsible for this energy transfer is called an excitation photon, with energy E_{excite} . While the electron is in the excited state, some of the energy is transferred to the system via non-radiative means which we label as $E_{non-radiative}$, leading to heating of the material. The amount of time the electron stays in this state is called relaxation time and is on the order of nanoseconds. When the electron finds its lowest excited singlet state it can fall to the ground state S_0 , while emitting a photon of energy E_f . If S_0 does not change, then the following must be true,

$$S_0 + E_{excite} = S_0 + E_{non-radiative} + E_{fluoresce} \tag{5}$$

$$E_{excite} > E_{fluoresce} \tag{6}$$

And combining equation 3 with equation 6,

$$\frac{1}{\lambda_{excite}} > \frac{1}{\lambda_{fluoresce}} \tag{7}$$

$$\lambda_{fluoresce} > \lambda_{excite}, \tag{8}$$

then the photon emitted must be of longer wavelength than the excitation wavelength. If all the energy goes to multiple non-radiative transitions without emission of a photon, then the material is simply heating up and no fluorescence occurs.

If we take the rate at which an excited system decays via emission of a photon and divide by the sum of all other non-radiative decays, it reveals a materials quantum yield. Fluorescence quantum yield is the efficiency with which a system can fluoresce. At a max of 1.0, the yield can also be stated as number of photons emitted per photons absorbed. (Lakowicz 1999)

This modified Jablonski diagram (Figure 1) shows graphically the concept of 1 photon fluorescence. Ground state, excitation, relaxation, then emission and so on.

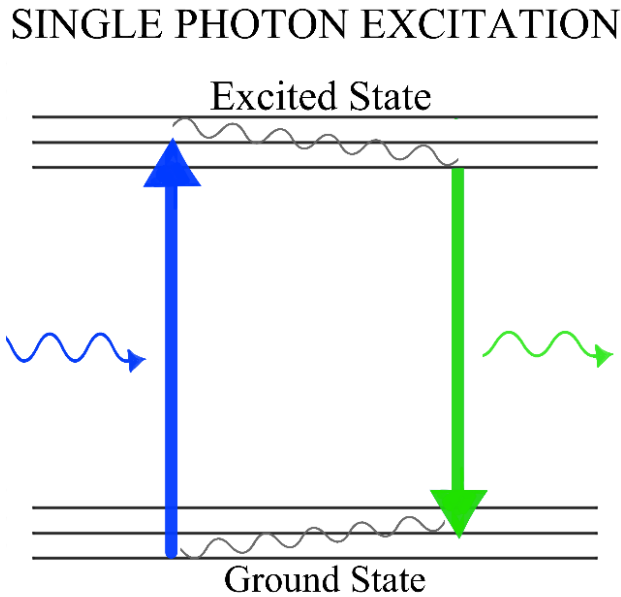


Figure 1: Modified Jablonski Diagram

2-PHOTON FLUORESCENCE

Maria Goeppert -Mayer had shown that when a single photon could be absorbed by a bound electron, there was some probability of the electron absorbing 2 photons instead. This is the case in 2-photon fluorescence, the excitation of the electron begins with the simultaneous absorption of 2 photons of any wavelength, depositing the sum of the photon energies into the system.

9

$$E_{excite} = \frac{hc}{\lambda_1} + \frac{hc}{\lambda_2}$$

In the laboratory the photons are created via a pulsed laser system. By definition, the photons are of the same wavelength, phase, energy, are coherent, and collimated. Fluorescence Experiments conducted in the photonics lab would be absorbing 2 photons of the same energy, and the absorbed energy would be twice the photons energy. In this case we can say that at excitation, the energy is,

$$S_0 + 2E_{2p}$$

The rest of the process to photon emission is the same as the fluorescence case. The same non-radiative transition occurs, followed by the electron falling to the ground state and emitting a photon. The difference being that the fluoresced photon energy is less than the sum of the energies of the excitation photons, and we can say,

11

$$\lambda_{fluoresce} > 2 \lambda_{2p}$$

2-photon fluorescence is said to occur when 2 photons are absorbed simultaneously, and one photon emitted that is of less energy than the 2 excitation photons summed. This modified Jablonski diagram shows graphically the concept of 2 photon fluorescence, ground state, excitation, relaxation, then emission and so on as shown in Figure 2.

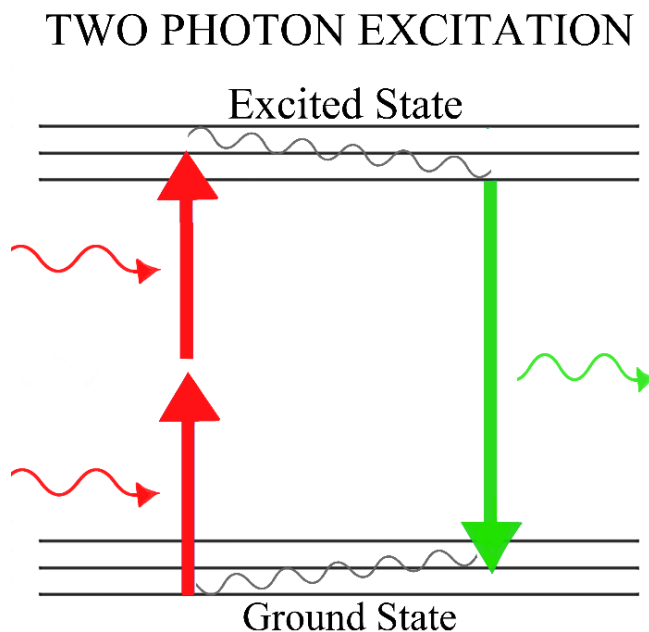


Figure 2: Two Photon Fluorescence Jablonski Diagram

Maria Goeppert Mayer stated that the probability of the 2-photon absorption occurring can be expressed as,

12

$$P_{2PA} \propto \sigma I^2$$

Where P_{2PA} is the probability, I is the intensity of the light impinging on the material, and σ is the unit of 2-photon molecular cross section (the Goeppert Mayer) that quantifies a molecule's propensity for 2-photon absorption. The unit is defined as $10^{-50} \text{ cm}^4 \text{ s} (\text{photon molecule})^{-1}$.

PHOTON CONFINEMENT

The high intensities of light required for 2-photon absorption can be achieved via 2 types of photon confinement, spatial and temporal confinement. The probability of a 2 photon absorption occurring is related to the 2-photon molecular cross section and the I^2 . Where the 2.P.M.C.S. is of on the order of 10^1 to 10^2 Goeppert Mayer, for typical fluorophores. And typical intensities required are on the order of 10^{28} photons $\text{cm}^{-1} \text{ s}^{-1}$ in order to begin the process of 2-photon absorption (Xu, Chris; 1996). The intensity of the Sun's photons at the Earth's surface on the same cross section and time scale is 10^{17} photons (Roberts, B.C.; 2017). In order to achieve 2-photon absorption an intensity of 100 billion times the intensity of sunlight is required.

Spatial confinement, also known as focusing, happens when the photons traveling through some cross-sectional area are converged to a very small spatial volume. Similar to how a magnifying glass concentrates the sun's rays. This increases the photon density at the focal point of the lens. The photonics lab uses a 1.2 numerical aperture objective lens in this role.

Temporal confinement, or focusing, happens when the photons produced in time are concentrated into smaller packets. Taking the photons that were produced and would have traveled over the course of sometime and compressing them into a smaller time. In the photonics lab this

is done by the Mai-Tai laser, taking the photons created in 1.25×10^{-8} seconds and compressing in into 100×10^{-15} seconds. A ratio of about 1:125,000.

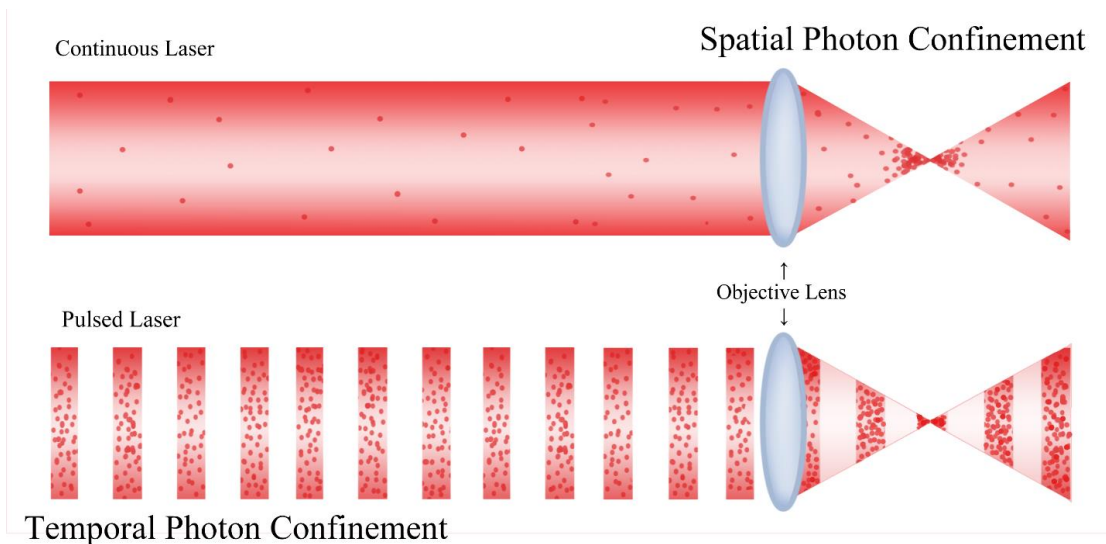


Figure 3: Temporal Photon Confinement

Combining these two photon confinement methods help to concentrate the photon density high enough to cross the threshold for non-linear optical processes. The two types of confinement are shown graphically in the Figure 3.

MAI-TAI

To achieve the photon density required a pulsed laser is used in conjunction with a high numerical aperture objective lens. The laser used in the photonics lab is a femtosecond pulsed Ti: Sapphire tunable laser source (Spectra-Physics, Mai Tai SP). Its pulse duration is about 100 fs with a repetition of 80 MHz. The wavelength of the laser is tunable from 690 nm to 1040 nm, with the maximum power up to 2.5 W. Given what we know, 80 million 100 fs pulses per second adds up to the laser sending photons only 0.08 % of the time. The laser is off the other 99.92% of the time.

It is a good thing to put this into human time scales. If we inflate the femtosecond to one second, then our 100 femtosecond pulse can be considered a 100 second pulse (less than 2

minutes). When the femtosecond scale is changed such that it becomes 1 second, then the 1 second scales to 31,709,791 years. This means that 1 second of femtosecond pulsing, at human time scales, means the laser would pulse for 100 seconds, every 4.7 months, for 31,709,791 years. Considering a typical experiment runs for 60 minutes, that scales up to 114,155,247,600 years. That is 100 Billion years longer than the age of the universe.

The benefit to the pulsed laser versus a continuous wave laser becomes obvious when you consider the intensities required to create the non-linear material response. If these intensities were delivered via continuous wave laser, the sample would burn. Having the pulses so far apart temporally gives the sample material time to absorb and dissipate heat without burning it. In addition, should an experiment require to capture millisecond, nanosecond, or picosecond resolution, the only way is to make the pulses smaller than the time scale of the event to be captured.

1-PHOTON VS. 2-PHOTON

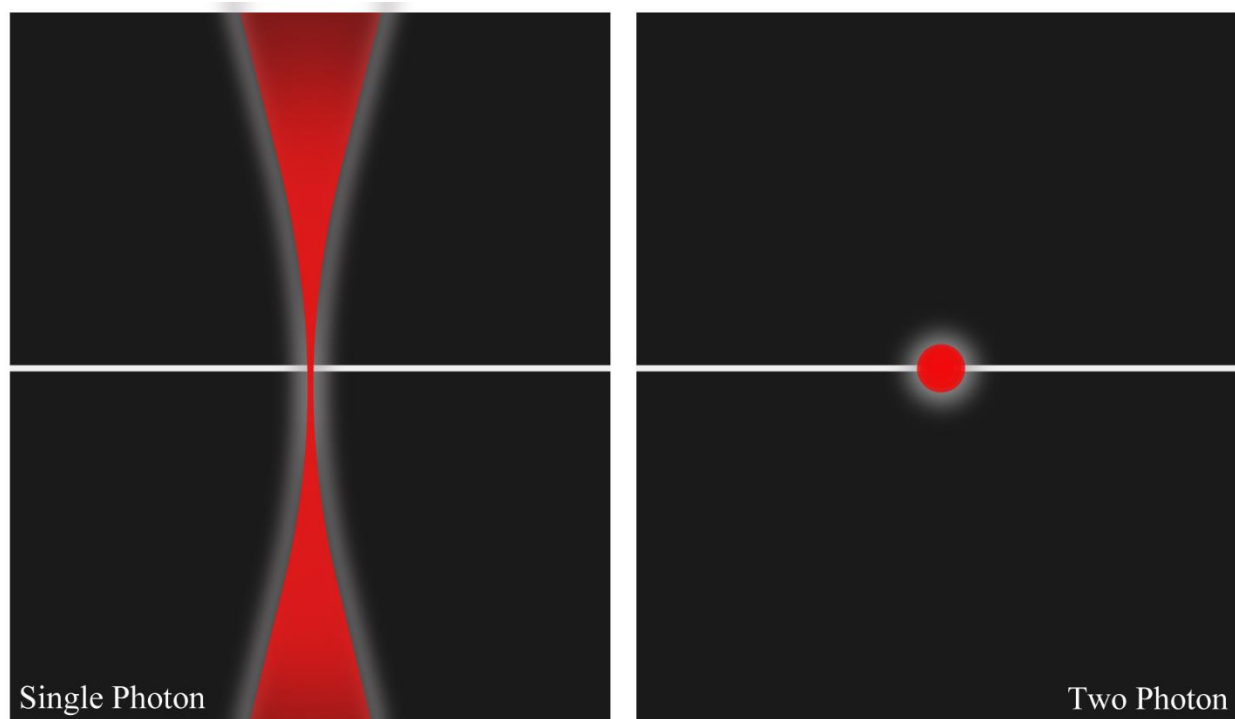


Figure 4: Single VS Two Photon

This Figure 4 represents a side view of the light exiting the objective lens, the difference between 1-photon excitation versus 2-photon excitation is very clear around the focal plane of the lens represented by the white line. In single photon excitation, as the light focuses, it forms what looks like an hourglass shape, everything inside this shape, everything the light touches, undergoes excitation. More excitations occur at the focal plane than out of the focus. That means that excitations outside the focus is non-zero. This is inconvenient for a multitude of reasons. The extra fluorescence adds to the background and noise of the experiment. Or, as is the case for the photo-cleaving experiment written about later in this dissertation, if the experiment calls for very specific, very small volumes to be illuminated by the laser, while also minimizing over exposure to the rest of the sample.

In 2-photon excitation, the only location that the sample can achieve the intensities necessary are where the two methods of photon confinement occur. That would be at the focal volume. Where the photons are confined both spatially and temporally. This focal volume is roughly $1 \mu\text{m}^3$ and located at the focus of the beam.

Chapter 2: 2-photon for Tissue Engineering

PHOTO CLEAVABLE MATERIALS PROJECT

The Ultrafast photonics lab would use a 2-photon microscope to characterize, and subsequently illuminate samples of a novel photocleavable material, in specific ways that would leave microchannels within a matrix of the material as a way of pre-vascularization. The resulting vascularized matrix could then be used to grow endothelial cells within the channels. Thus, leaving an engineered tissue that would allow and promote new cell growth. With the goal of creating stackable blocks of said material.

TISSUE ENGINEERING

Every day, all over the world, hospitals replace or attempt to repair tissues that have been damaged, destroyed, or degenerated. An engineered tissue uses the body's cells, in a created scaffold, with the right materials and environment that promotes growth. These make up the tissue engineering "Triad" required for successful tissue integration. The scaffold is the 3 dimensional matrix in which and through which the cells will grow and create a tissue. The cells, are whatever type of cells are to be seeded into or onto the matrix. The signals are things like growth factors that encourage the growth and proliferation of cells and tissues. Each of these three must be carefully considered and custom tailored for each specific tissue application. (O'Brien 2011).

Even a perfectly tailored engineered tissue faces the problem of vascularization. If an engineered tissue is to survive as a viable tissue alternative, then it must survive long enough for the cells to proliferate through the matrix. Unfortunately, without delivery of oxygen and nutrients to all parts of the engineered tissue, it would die relatively quickly.

PRE-VASCULARIZATION

Pre-vascularization, Or rather the lack of vascularization is a significant hurdle to tissue engineering. Even with a perfect tissue replacement, the body must vascularize the tissue replacement in order to deliver nutrients, oxygen, signals, etc. to the tissue. Without the pathways the new tissue will die of hypoxia. The body is limited to a maximal growth rate of 100 to 200 μm per week. As a comparison, skin is 2,000 μm thick (Utzinger, U.; Baggett, B.; Weiss, J.A.; Hoying, J.B.; Edgar, L.T. 2015). Even larger tissue replacements would suffer even larger losses. It is necessary to vascularize the scaffold.

Two strategies are common to spur vascularization, stimulating Angiogenesis and pre-vascularization. Angiogenesis is where the environment within the tissue is manipulated to get maximum vascular growth. Using growth factors to signal to the seed cells to grow into the engineered tissue (Utzinger, U.; Baggett, B.; Weiss, J.A.; Hoying, J.B.; Edgar, L.T. 2015). However, this is still limited to the cell's growth velocity into the scaffold. The second method is to leave microchannels within the tissue matrix, then grow vascular pathways in them via cell seeding, spheroids, or cell sheet technology. These microchannels mimic vasculature that the body can then attach to, in order to keep the tissue alive (Laschke, M.W.; Menger, M.D.; 2012) .

It is the intention of the project to pre-vascularize an engineered tissue scaffold created with the express purpose of using the photonics group's 2-photon microscope to create the microchannels via a photo-cleavable molecule incorporated into the engineered tissue, such that exposure at the intensities of the 2-photon rastered laser will leave the matrix intact while only breaking down the material where the endothelial cells will grow. (Akter 2016)

PHOTO-REACTIVE COLLAGEN-LIKE PEPTIDES

In order to pre-vascularize an engineered tissue with the 2-photon microscope, a novel material would have to be created that was non-linear in photon absorption, photo-cleave during a 2-photon absorption, be a suitable matrix, be non-toxic to cell growth before and after photo-cleaving, be suitably transparent to allow passage of light internally, and robust enough to survive normal laboratory handling.

N-acyl-7-nitroindoline was investigated as a possible photo-reactive molecule. Previously used as a molecule to cage other reactive molecules, it would release the caged molecule when exposed to 350nm light. This nitroindoline molecule could be incorporated into a molecule thus making it photo cleavable. Dr. Alfredo Ornelas was able to synthesize a collagen mimicking peptide sequence, which consisted of 5 hexapeptide sequences, and 4 of the photoreactive moieties. The peptide sequences were composed of glycine, proline, hypoproline. The moieties were a photo reactive N-peptidyl-7-nitroindoline. Together they compose a 34-mer polypeptide that can crosslink to create a hydrogel. (Ornelas, A.; Paez, A. 2018) Shown in figure 5, is the peptide sequence that was created. Cleavage points are between the glycine and nitroindoline molecule (Hatch, K.A.; 2016).

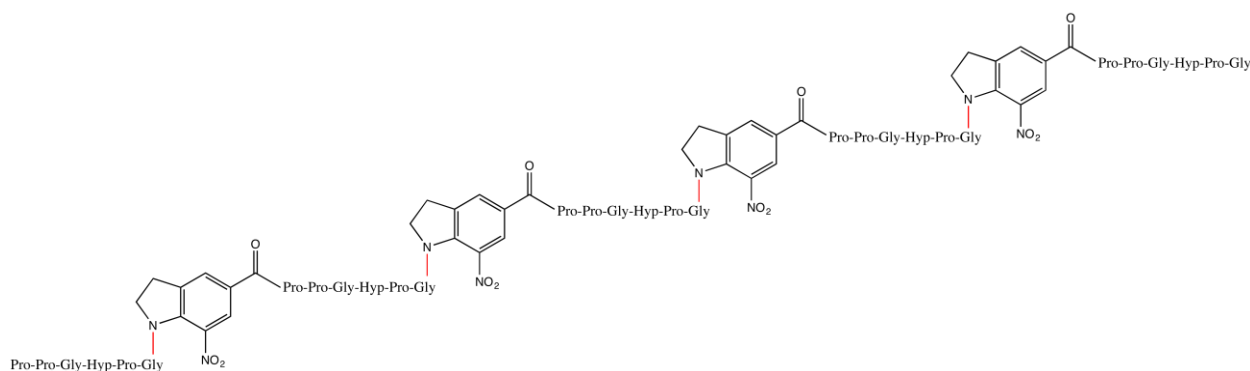


Figure 5: Peptide Sequence

2-PHOTON MICROSCOPE

The 2-photon microscope is a custom-built microscope in the photonics lab. It is typically used to image and characterize materials, cells, nano-particles etc. The power produced by the Mai Tai laser is approx. 2.5 watts and polarized horizontally. Followed by a pair of optical components, the waveplate and polarizer, serve to limit the power of the beam and make the power tunable. The linear polarizer selects one polarization of light to allow through. The waveplate serves to rotate the polarization. The amount of laser light that gets through is defined by Malus law, that outgoing intensity is equal to incoming intensity $(\cos \text{ of the angle between them})^2$. Photo-Diodes are used with synchronization of all the timing circuits. The polygonal mirror is a 36 faceted mirror that spins at 480 revolutions per second, that scans horizontally. A mirror galvanometer (galvo) is a small mirror that can vibrate at various frequencies. This galvo mirror's frequency is 30 Hz. Between the two, the laser beam is rastered and sent through the objective lens where it illuminates the sample. In most imaging cases, the sample absorbs 2 photons and then fluoresces. The fluorescence photons return through the same objective and are diverted to RGB photomultiplier tubes.

Parameters that can be controlled on the 2-photon microscope include; laser wavelength, laser power, polarization, photomultiplier tube driving voltages, image averaging, precision stage controls of X Y and Z, with the ability to take images, videos, Z-scans for 3d imaging, and longtime exposures of materials.

DECAY

Given that a collagen like peptide, or any molecule, can photo cleave during a 2-photon absorption, observation of a sample being illuminated with high enough intensities will begin to show decay of the fluorescence. The data is collected via multi-channel images taken every few

minutes showing that the fluorescence intensity drops with time. However, it may be noted that if a sample is fluorescing, can it be cleaving? The probability of cleaving cannot exist until the probability of 2-photon absorption is satisfied. Therefore, a sample that is being illuminated, first has a probability of 2-photon events, and of these systems that are now 2-photon-active, there is some percentage that will fluoresce and some that will cleave. Given that some time passes and there are fewer available systems within the sample to become 2-photon-active, then there must be less fluorescence and less photo-cleavage as time goes on. Our goal then becomes to prove that the decay rate is contingent on the first part of this, the probability of systems that can become 2-photon-active.

Previous work was able to show the fluorescence decay of lyophilized peptide dissolved in water (1 mg to 2 ul) creating a thin film of the peptide on microscope slide glass. Different spots on the film were exposed to 710 nm light, each with a different power. Beginning at 100 mW up to 200 mW in 25 mW increments. Plotting the normalized fluorescence intensity versus time shows this decay. The curves were fitted using an exponential decay regression fit from MATLAB of the form;

13

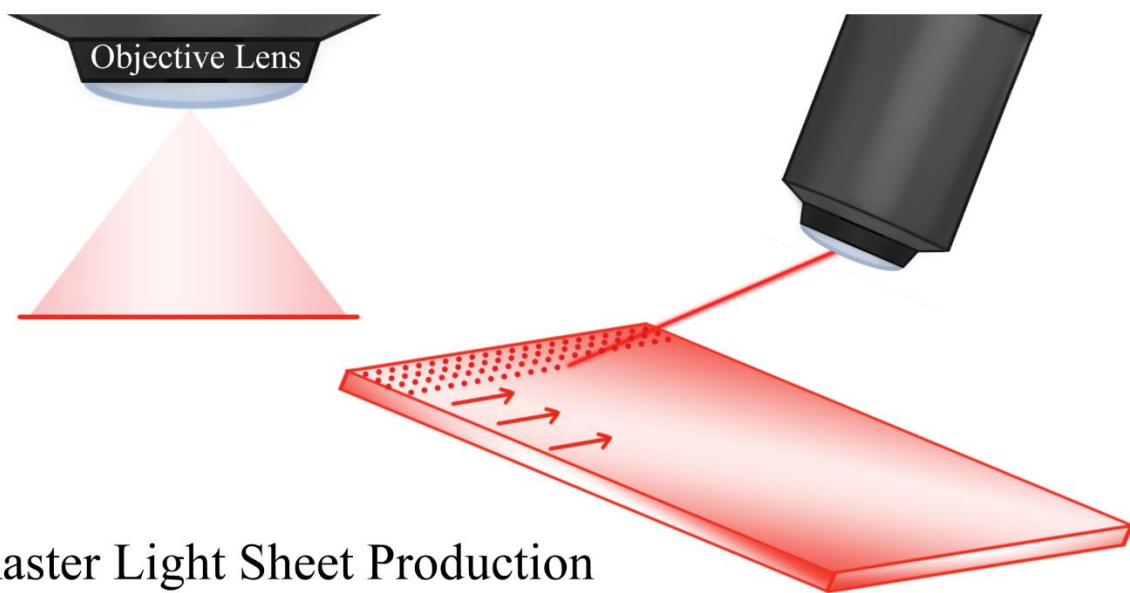
$$F(t) = F e^{-\beta t}$$

Where beta is the fluorescence decay rate, which also tells us about the photo-cleaving reaction rate. We can assume this because the only wavelength the sample is exposed to (710nm) can only provoke the cleaving of the peptide if 2-photons are absorbed. Single photons of this light can not provoke the reaction to occur. Plotting this rate versus intensity as a double log plot, creates a linear graph with slope 2.007. This supports that the peptide was cleaved as expected. This was later confirmed via mass spectrometry. (Hatch, K.A.; Ornelas, A.; Williams K. N.; Boland, K.;

Michael, K.; Li, C. 2016). Using this approach, we can prove that a sample is decaying due to a non-linear process.

UTEP LOGO MASK

Due to the eventual requirement of the photocleavable material experiment to leave blood vessel like channels within the material, it is necessary to demonstrate that the 2-photon microscope can expose the photo-cleavable material in a repeatable and controlled manner. One of the goals of the project is to leave a $50\ \mu\text{m}$ by $50\ \mu\text{m}$ channel within the matrix of the engineered material. The focal plane that is created by the 2-photon microscope is a $300\ \mu\text{m}$ by $300\ \mu\text{m}$ by $1\ \mu\text{m}$ sheet of light normal to the propagation direction of the light, see Figure 6.



Raster Light Sheet Production

Figure 6: Raster Light Sheet Production

A proof of concept was required to demonstrate that the light sheet could be manipulated in such a way that to expose the sample in the patterns necessary for vascular imitation. Vascular structures can be as small as $10\ \mu\text{m}$ in diameter up to $100\ \mu\text{m}$ in diameter (Unekawa; et al. 2010). This proof of concept took the form of a mask that can be placed at the intermediate focal plane,

before the objective lens, see Figure 7.

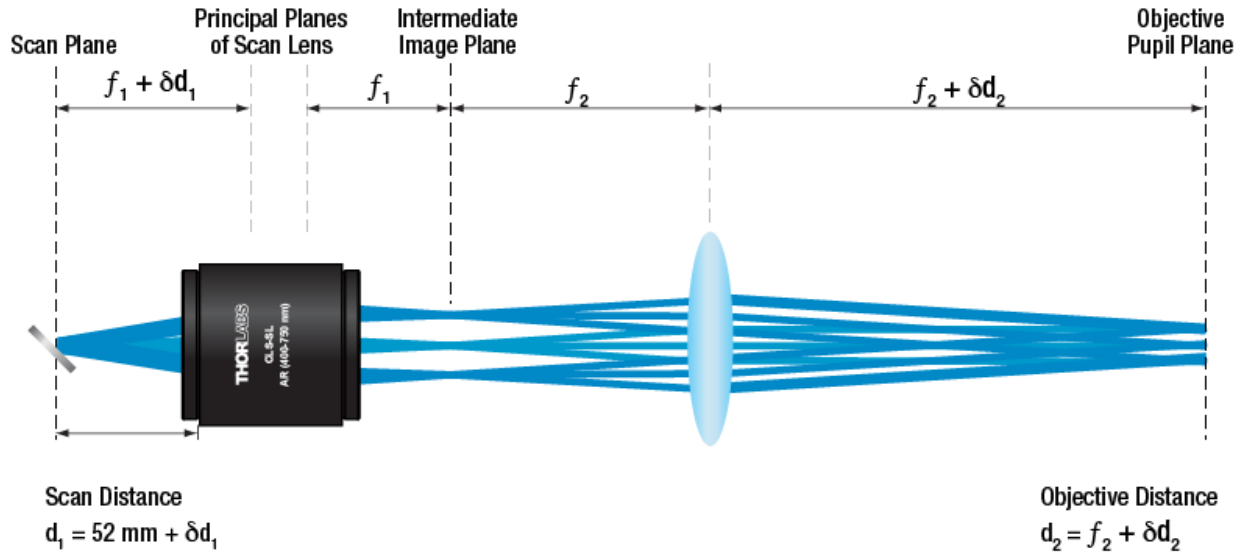


Figure 7: Demonstration of where the intermediate image plane is.

Whatever shapes are on the mask that is placed in this position, would be projected onto the sample on the stage. All statistics and optics data can be taken from the exposed area, while protecting the rest of the material from exposure to the laser beam. From previous published results, it is known that the linker molecule has a change in appearance when exposed to 710 nm light (Hatch, K.A.; Ornelas, A.; Williams K. N.; Boland, K.; Michael, K.; Li, C. 2016). It becomes noticeably darker. The mask proof of concept needed to show that we could do the following;

1. Create patterns on the material
2. Make the patterns sufficiently small (between 10 μm to 100 μm)
3. That the peptide material was reacting as before

Using a piece of glass, electrical tape, clamps, a white light microscope, and an X-acto knife, the mask was created. The UTEP logo shown in Figure 8 is less than 1 cm across. Placing this mask at the intermediate focal plane allowed for the projection of the UTEP logo onto sample

stage. The holding mechanism for the mask was a rotating stand and clamp that would allow for the mask to be rotated into and out of position easily. When the mask was out of position it allowed for un-restricted exploration of the sample and a wider field of view. The mask in the in position created the pattern at the focal volume.



Figure 8: UTEP LogoMask

A 10 μ l sample of fmoc-gly-bni (a suitable test molecule for the nitroindoline linker molecule) in solution was placed on a slide and allowed to dry, which created a film of material with a uniform surface. This film was covered with a cover glass and tape to protect from water intrusion and minimize evaporation. Once on the stage, the sample was moved in z and the surface of the sample was located. A search by scanning across the sample quickly to avoid over exposure to the laser and cause undesired decay, a good location for the logo was found. Sample coordinates were taken for the potential exposure site, then the sample moved out of the focal volume of the laser in order to prevent exposure and undesired decay. The mask was rotated into place and the

sample returned to its original z , in order to assure that the focal plane was directly on the surface of the film. It is critical that the focal volume, which is approx. $300 \times 300 \times 1 \mu\text{m}$, be co-located at the very top $1 \mu\text{m}$ of the material.

The Mai Tai was tuned to 710 nm , with a power of 75mW , and time of exposure was 60 minutes. Images were taken every few minutes. These series of images (Figure 9) show from time zero to 60 minutes.

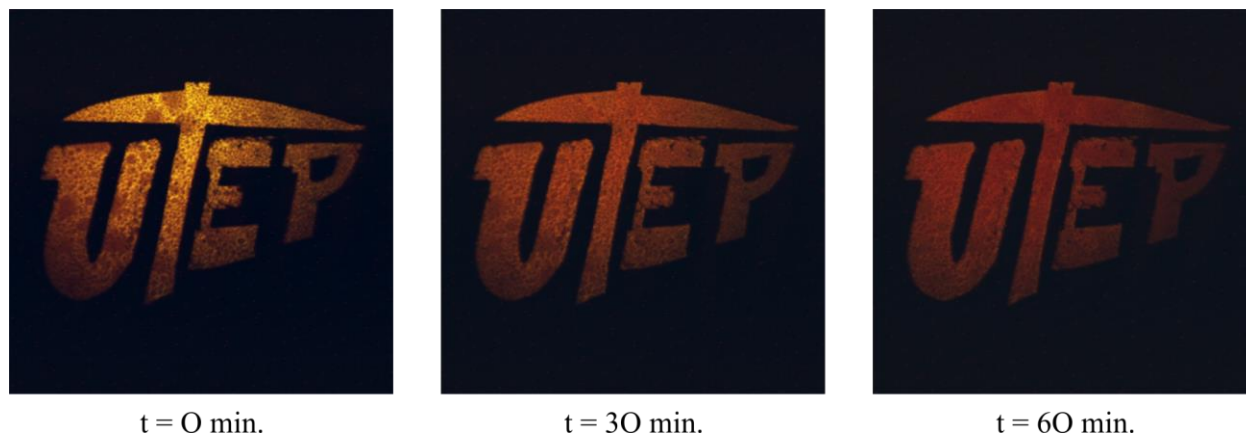


Figure 9: UTEP Logo at Different Exposition Times

Intensities were extracted from image files with ImageJ then plotted to verify fluorescence decay. After 60 minutes of shining the laser through the mask and onto the sample, the mask was rotated out of the way and an image taken to verify that fluorescence had decayed in the logo but had not decayed in the mask's negative space, see Figure 10

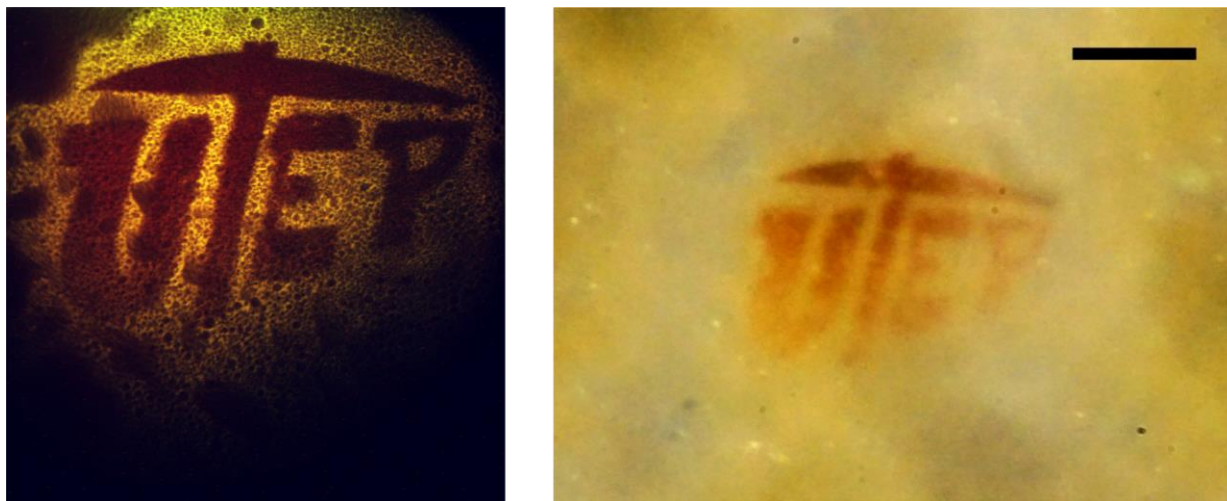


Figure 10: Fluorescence Decay examples post illumination

The UTEP logo mask experiment showed that a mask at the intermediate focal plane could effectively expose specific areas of a sample, while also blocking exposure to other areas. In addition, the UTEP logo had features that were of varying width and length, showing that features down to $10\ \mu\text{m}$ were feasible. This also proves that the 2-photon microscope can be modified via mask to produce any type of 2-dimensional pattern, with features smaller than $10\ \mu\text{m}$. Also that no leakage of the laser light occurred into the dark surrounding areas of the mask.

PEPTIDE HYDROGEL PHOTO-CLEAVING, A TYPICAL CASE

Experiments would be conducted on many different samples. The chemistry group would bring a peptide sample in the form of a hydrogel to the photonics lab. Samples would be evaluated for viscosity, hardness, workability, and each samples likelihood of being able to form a microchannel in the hydrogel and survivability under the laser illumination. Samples were then cut, mounted on glass slides, isolated from the local environment, and prepared as appropriate for exposure on the 2-photon microscope. Occasionally, samples would be taken back to the chemistry lab and re-worked to return as a new sample to be irradiated.

Throughout the development of the samples, different masks were created. Tree masks,

grid masks, shaped masks, each made as the experimental parameters dictated. The development of the tree mask stems from the necessity to mimic blood vessels branching off from a major vessel. As such a mask was created and proved to be able to photo cleave the hydrogels produced with sufficiently small features, see Figure 11.

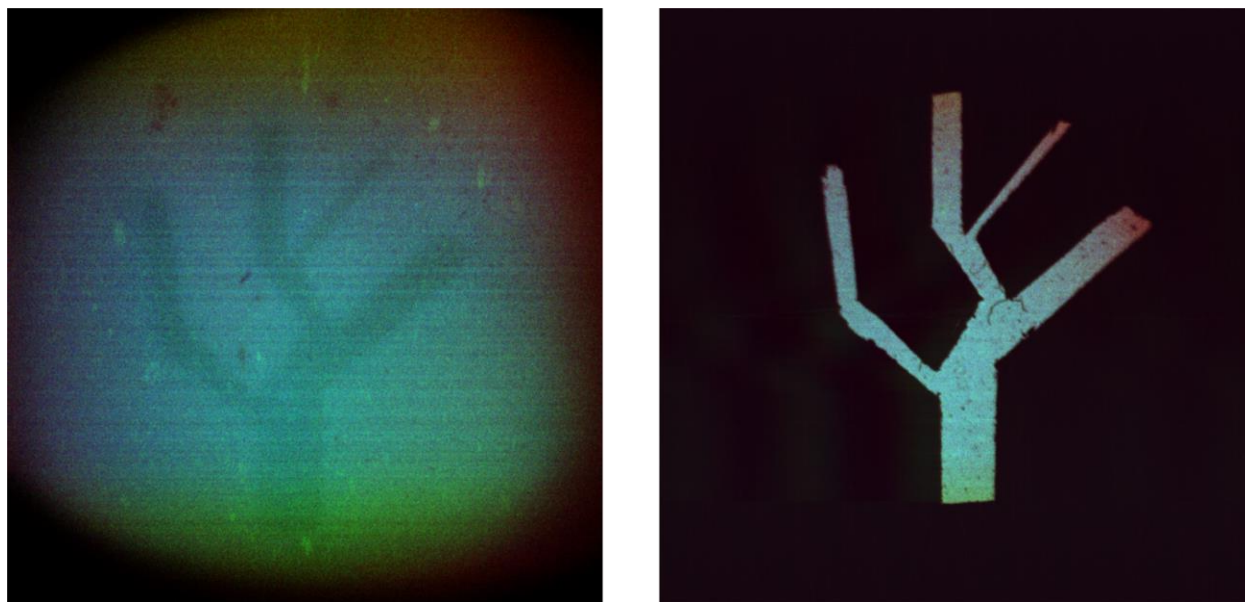


Figure 11: Tree Mask & Exposition

In the case of Sample 18's "pinstripe mask" the goal of the experiment was to create an area of photo-cleaved hydrogel with many parallel microchannels, as proof of concept that channels could be carved into the sample. To which this mask was created, see

The experimental parameters required that the illuminated spot be easily accessible and easily located post exposure. This led to the creation of the pinstripe mask with a large square area in the middle of the mask. The idea was that post illumination of the sample, if 2-photon photo cleavage occurred, and there was a 300 by 300 μm area of parallel channels, it would make location of the channels and subsequently, locating the square of illuminated material, easier.



Figure 12: Pinstripe Mask

PEPTIDE HYDROGEL: AREA OF INTEREST

As shown in Figure 13 due to the focal light sheet of the 2-photon microscope being shaped as a plane perpendicular to the objective lens (z propagation direction of the beam), in order to illuminate the surface of the sample, the sample itself must be as flat and uniform as possible. If the sample topography is too bumpy, then regions of the sample would be above and over the light sheet. In order to create the best possible scenario for leaving a “flat” surface, a “double cutting tool” was created in the photonics lab that would cut a “large sample” into a smaller sample.

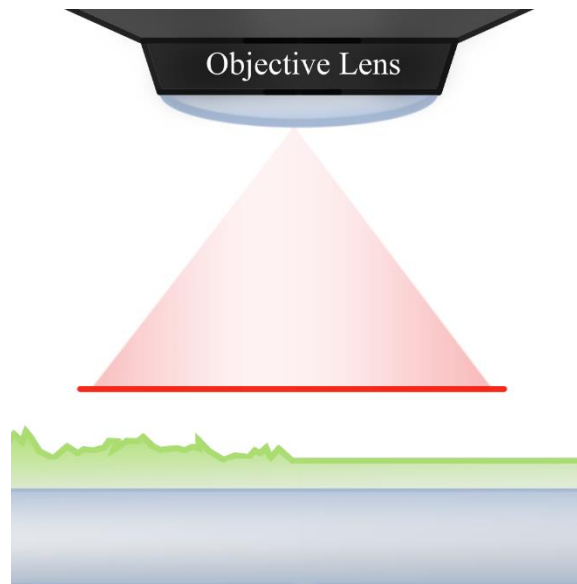


Figure 13: Focal Light Sheet Diagram

The double cutter tool was created using two razor blades clamped together with a 1.0 millimeter spacer between them. This created two parallel cutting surfaces that left the hydrogel with two smooth surfaces. Before cutting a sample, the double cutter tool was disassembled, each part was washed in acetone, and wiped with a laboratory wipe, then the tool was reassembled. Before cutting the sample, the double blades were dipped in distilled water. This coating of water made it easier for the material being cut to slide off the blades after cutting. To release the freshly cut sample the double cutter was disassembled, and the sample pushed off the blade onto a prepared slide. After illumination the sample was to be imaged via AFM or SEM and required that it be mounted on a conductive surface, therefore the slide was prepared, prior to cutting the material, with a conductive carbon adhesive, and a fiducial marker in the form of a white arrow sticker butted up to the sample, and careful cataloging of internal structures in the sample, see Figure 14.

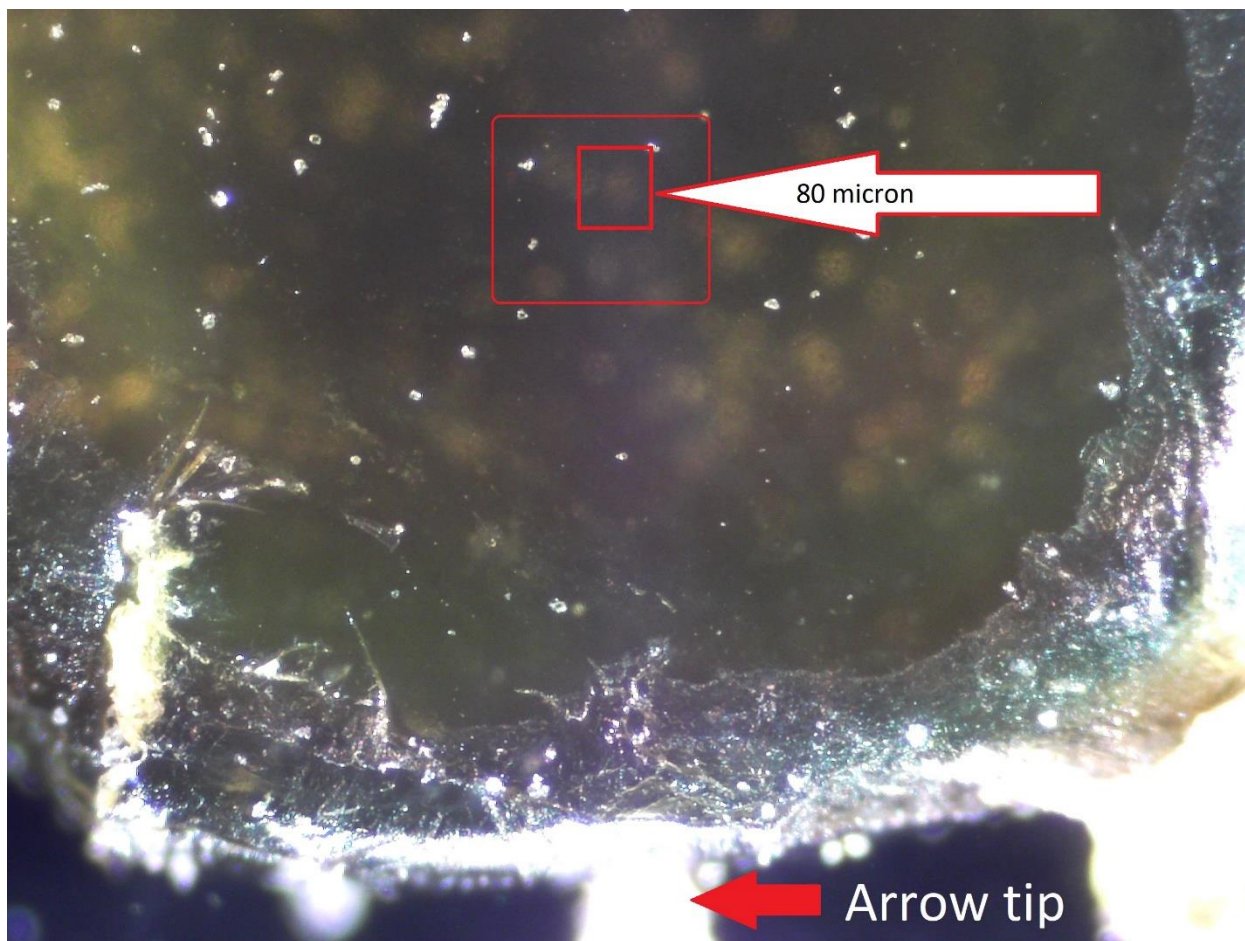


Figure 14: White light image of HydroGel, post 2-photon illumination.

In order to minimize water loss during illumination, a chamber was built up around the sample using multiple layers of adhesive tape topped with a cover slip. White light images were taken for ease of locating the illuminated spot, by either of the teams.

PEPTIDE HYDROGEL: 60 MINUTE ILLUMINATION

The sample was mounted onto the 2-photon microscope stage. The surface of the sample was brought into focus, then the photo-multiplier tube driving voltages were adjusted as needed, and the stage position was noted. The sample was lowered away from the focal plane and the pinstripe mask was lowered into place. Care was taken to verify that the pinstripes of exposure ran

perpendicular to the cutting direction, this helped to eliminate confusion that could occur if there were imperfections in the blades cutting surfaces that would leave striations on the material.

The experiment would run 60 minutes of illumination, with images captured every five minutes. After 60 minutes, the stage was moved 1 μm closer to the objective, to create a deeper exposed area that would be easier to identify using AFM and SEM. This would be repeated until a 3 μm deep layer of sample was illuminated. Upon removal of the mask, a 2-photon image of the sample shows that there was photo cleaving on the sample surface due to the laser. Removal of the mask showed that the sample was no longer fluorescing in the exposed areas, see Figure 15.

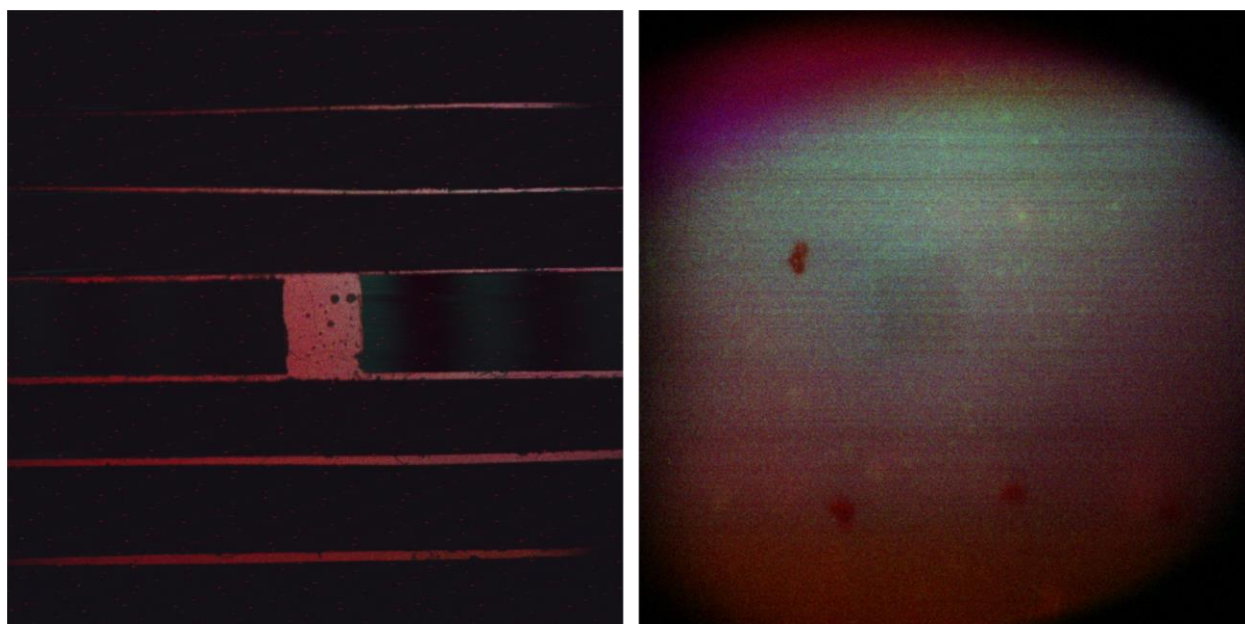


Figure 15: Mask Removal Fluorescing

Post-illumination white light images could not pick up on the subtle difference of a 3 μm deep photo-cleaved sample. This is shown in Figure 16.

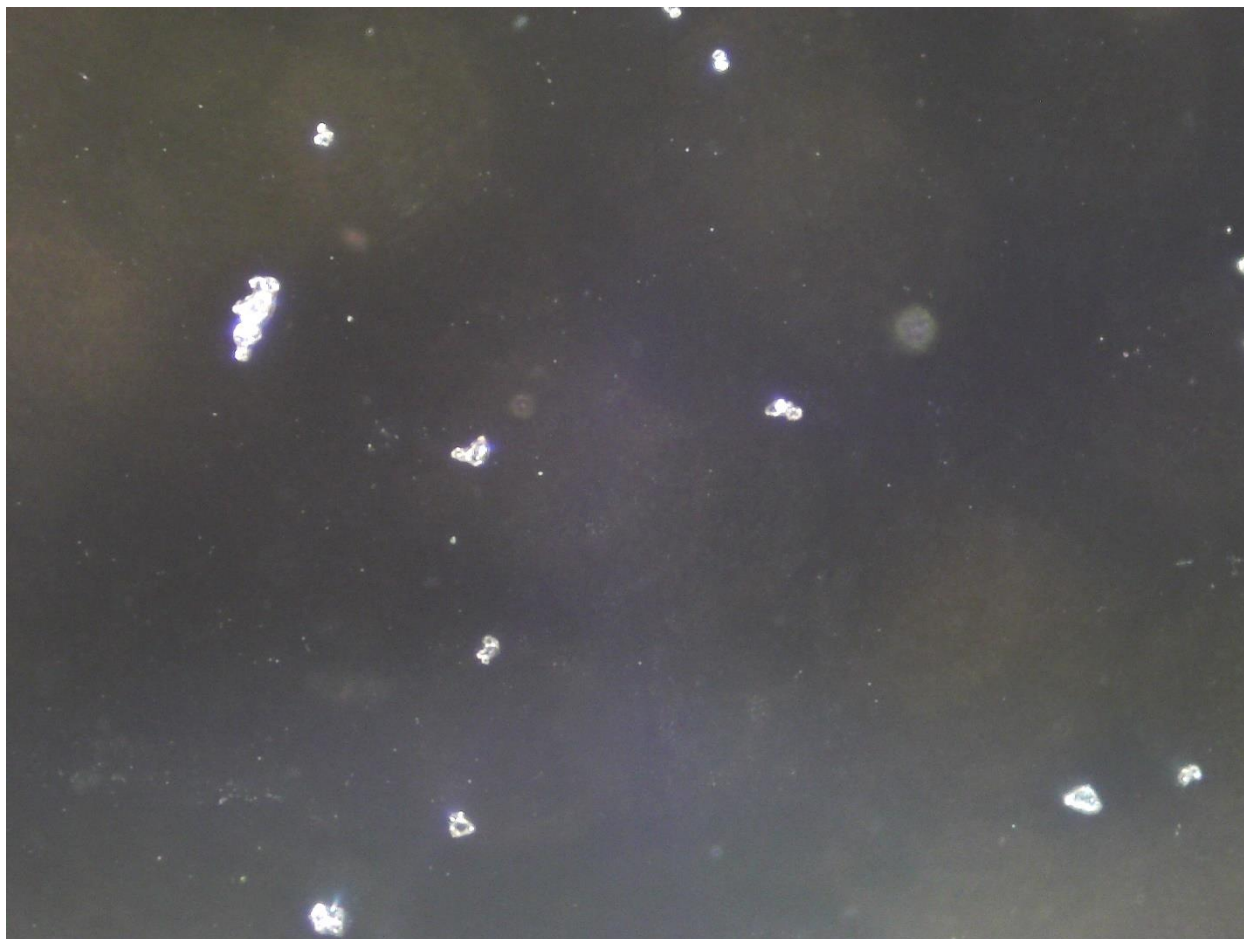


Figure 16: Post Illumination Sample

AFM and SEM proved inconclusive at finding the small features left on the surface of sample 18.

NON-LINEAR OPTICS OF NEW MATERIALS

Although use of the nitroindoline molecule as a linker for the peptide chain had shown promise, a novel use for the Nitroindoline molecule had been investigated that would be more efficient, cheaper and faster. This has led to the development of 3 new materials that require the same characterization as the peptide. The chemistry group was able to create new molecules that use nitroindoline within them in order to have the photo-cleavable property. These new molecules

are cheaper and easier to produce and as such their non-linear properties were explored, alongside a reference nitroindoline molecule. These molecules are:

1. BNI – Amide (Reference)
2. BNI – Benzylamine Urea
3. BNI – Benzylalcohol Carbamate
4. BNI – Ethanethiol ThioCarbamate

Each of these samples was illuminated with the 2-photon microscope, decays calculated, and ranked, following prior work protocols from the peptide cleaving experiments.

The chemistry group would provide samples prepared on a thin layer chromatography (TLC) chip in the same way as is done for their single photon fluorescence experiments. A solution of the sample dissolved in acetone would be created, then a capillary tube is touched to the surface of the solution, and subsequently touched to the TLC chip with attention paid to creating a uniform even surface. These would be provided the same day the photonics group would be checking non-linear behavior.

The photonics group would use the 2-photon microscope to illuminate the samples. Standardized procedure is as follows.

TLC chip with sample is placed on a microscope slide and covered with a coverslip. The edges of the cover slip are covered in tape to prevent water from entering the sample area. The microscope was powered up and parameters set according to the sample involved. Once an image of the fluorescing sample is obtained, photo-multiplier tube driving voltages are adjusted to keep all 3 channels from saturating the pixel values in the images produced by OMCenter. Once a good location is selected, a shape mask is rotated into the intermediate focal plane of the objective and a sequence of images is taken. Depending on the sample and decay rates expected this can vary

from 60 minutes to 180 minutes, with images taken every 5 minutes. Once the images are obtained, they are processed through ImageJ, where the channels are split from one another, regions of interest defined, and intensity values taken for each image. With this data a fluorescence intensity versus time graph can be created. This process is then repeated 6 – 8 times, each time increasing the power of the laser by 5, 10, or 20 mW depending on the sample. Meaning that for long exposure time experiments the total run time can be upward of 24 continuous hours on the microscope. Each run at each power has its own intensity decay curve. An exponential regression line fit is done for each of these, then these data values are graphed in a double log plot of beta (decay) versus power. This serves to prove that indeed the process causing the decay is due to the non-linear 2-photon process. Once all samples are illuminated and data captured and processed, the sample's decay rates can be compared and a “best sample” can be chosen. In this case the BNI-amide is kept as a reference material and plotted against the potential new materials.

RESULTS

With the 34-mer peptide, the experiments have shown that a photo-cleavable molecule could be created that could create a 3dimensional scaffold that could then be exposed to high intensity pulsed laser light that would provoke a cleaving of the molecule. Additionally, the material was shown to be cleaving as expected leaving behind several types of cleaved peptide lengths. It was shown that the illumination could be controlled to create features on the material that would be less than 10 μm in width. Also that appropriate patterns were able to be left on the and in the material.

With the new crosslinker type nitroindoline derivatives, it was shown that BNI-amide, the reference molecule, decayed the fastest, followed by the BNI-thiocarbamate. The BNI-carbamate

and BNI-urea are photo-cleaving at rates that place them in a slower regime of decay. A combined plot of all for molecule decay curves for 150 mW is shown in Figure 17

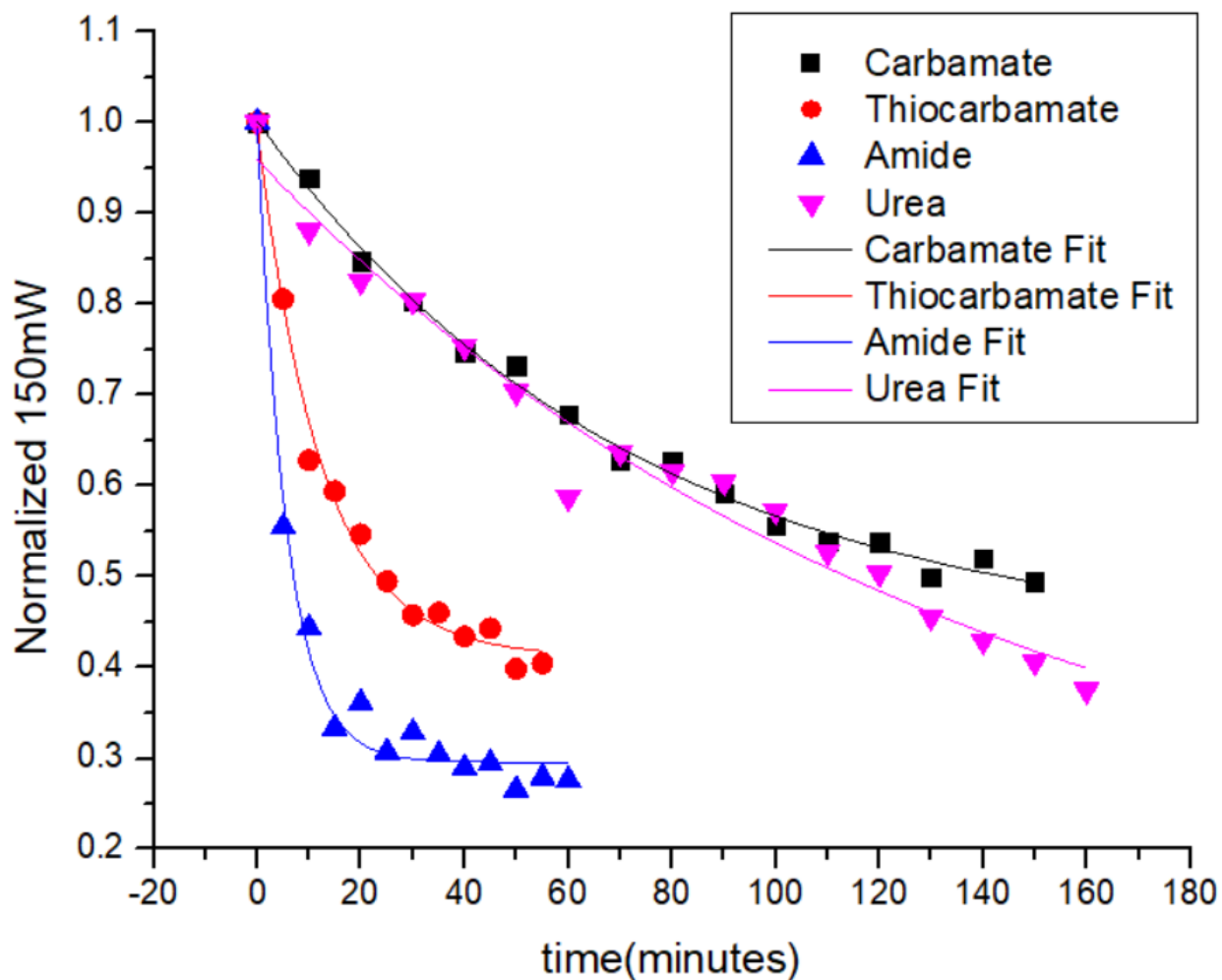


Figure 17: Molecule Decay Curves for 150 mW

Table 1 shows the decay constants for all 4 molecules at 150 mW. The amide reference being the fastest at 0.175, followed by thiocarbamate with half that, then the carbamate at 0.0138 followed by the urea molecule decay constant at half that of carbamate.

Table 1: Decay Constants for different materials

Material	Decay Constant
Amide	0.175
Thiocarbamate	.0815
Carbamate	.0138
Urea	.0074

Although velocity of reaction is the driving factor, it may occur that one of the slower molecules will be much more efficient at crosslinking. This project is part of a combined initiative of an interdisciplinary team of labs with goals and experiments that will continue after my participation and contribution ends. After characterization of photo-cleaving and fluorescence decay, a 3d material must be created that must then be pre-vascularized. Other approaches and materials are also being developed and pursued.

Chapter 3 Flow Cytometer using Non-Diffracting Light Beams

FLOW CYTOMETRY

Flow Cytometry is the act of counting cells in a flowing media, much like blood cells flow inside an artery. The counting of cells can be in vivo or can be blood cells flowed through a manufactured microfluidic channel chipset. A flow cytometer is typically composed of a laser shining through a micro fluidic stage, with detectors that can amplify weak signals. Cells of interest are flowed in media through the microfluidic channel such that they intersect the laser beam. The cells are typically tagged or stained in order to fluoresce under the laser light. This technique is used to physically sort cells, to count cells, for biomarker detection, and even diagnosis of health conditions like cancer. (Givan 2010). A flow cytometer is like a microscope that reports a counted cell as a spike of fluorescence at certain wavelength, width, and intensity. Careful characterization of the cells to be counted is required for best optimization of the flow cytometer function.

PROJECT DESCRIPTION & UNIQUE PROBLEMS

Although in vivo flow cytometry is an emerging technology and important biological tool for cell counting, and diagnostic purposes, that has research behind it, it is not without its own unique challenges. The concept of scanning a beam of light across a vein or artery to create a light sheet that can illuminate a passing cell is simple enough. However, given the penetration depths of typical light-sheet-based flow cytometers, the experiments are limited to very shallow and superficial venules, often found in the eye or ear. Using the near infrared portion of the spectrum for multiphoton excitation offers better penetration depth. A penetration depth of 1.4 mm into mouse brain tissue was achieved using this technique (Horton, N.G; et al. 2013) It is an obvious solution to apply 2-photon fluorescence to the existing in-vivo flow cytometer research (Kong, L.; Tang, J.; Cui, M. 2016). However, in order to achieve the high intensity values required to provoke

2-photon fluorescence, a focused gaussian beam is used. As was shown previously the volume of 2-photon excitation in this experimental setup can be thought of as a sub- μm cube at the focus of the gaussian beam. Scanning this across the blood vessel limits the effectiveness of detection. Instead of creating a light sheet, it creates a scanned $1 \mu\text{m}$ volume across the blood vessel effectively creating a line in 3 dimensional space that can go through the middle of vascular pathway. This line of 2-photon excitation is $1 \times 1 \times 100 \mu\text{m}$. A typical blood vessel can vary between $10 \mu\text{m}$ and $100 \mu\text{m}$ in diameter. Cells are typically on the order of $7 \mu\text{m}$ in diameter. As the vessels grow larger cells can pass over or under the scanned beam and would not fluoresce. Efficacy of this technique drops quickly for larger blood vessels as less of the cross-sectional area is sampled (Figure 18).

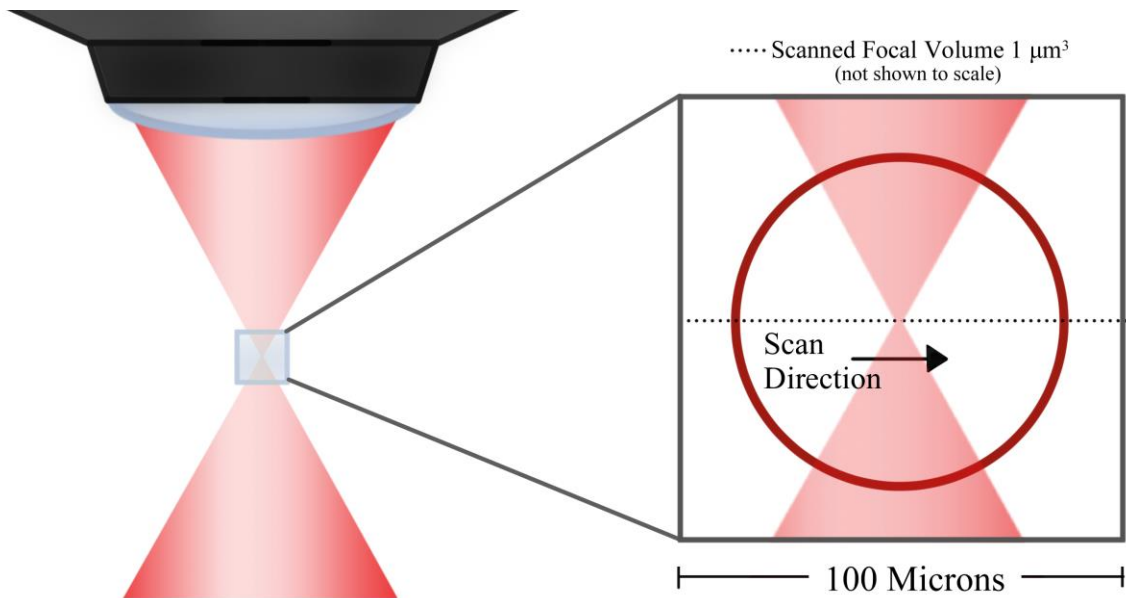


Figure 18: Cross-section Diagram: scanned focal volume through vascular pathway

In this regard the benefit of the 2-photon penetration depth is negated. However, if we could extend the focal volume of the 2-photon excitation to be longer in the z-direction then the light sheet created would be more and more efficient and cover the cross-sectional area of the

blood vessel. when comparing to a tight gaussian focus. In order to extend that focal volume, the researcher would have to use a type of light beam that would not diffract. Non-diffracting light beams are the subject of the next section.

Also challenging is that circulating tumor cells can be very diffuse. They are extremely rare, in some cases 1 cell every few minutes. These cells are the type that are normally associated with metastasis. With such low cell counts per blood volume, even classic cancer detection such as drawing blood and then analyzing blood could create a false negative for various reasons. The advantage of the in vivo detection is sampling of the blood volume in the live animal would be that the blood is kept alive, and the full body is sampled every few minutes as blood recirculates naturally (Tan 2019).

Another challenge has been the low fluorescence response of tagged cells in vivo, in addition to the flow velocity of fluids in blood vessels. The well-known metric for blood flow and detection is that a tagged cell will pass a $100\ \mu\text{m}$ by $100\ \mu\text{m}$ area at a velocity of approximately $1000\ \mu\text{m}$ per second. This means that 2-photon absorption, fluorescence, and detection must happen at the millisecond time scale. Many 2-photon fluorescence experiments rely on long time exposures in order to increase the signal to noise ratio. This is no longer an option for in-vivo flow cytometry (Pons 2019). As such the lab's approach is a combination of hardware optimization, hardware sensitivity and post processing code taking advantage of the ability to scan at rates that oversample and then use that to the advantage of the experiment.

NON DIFFRACTING BEAMS

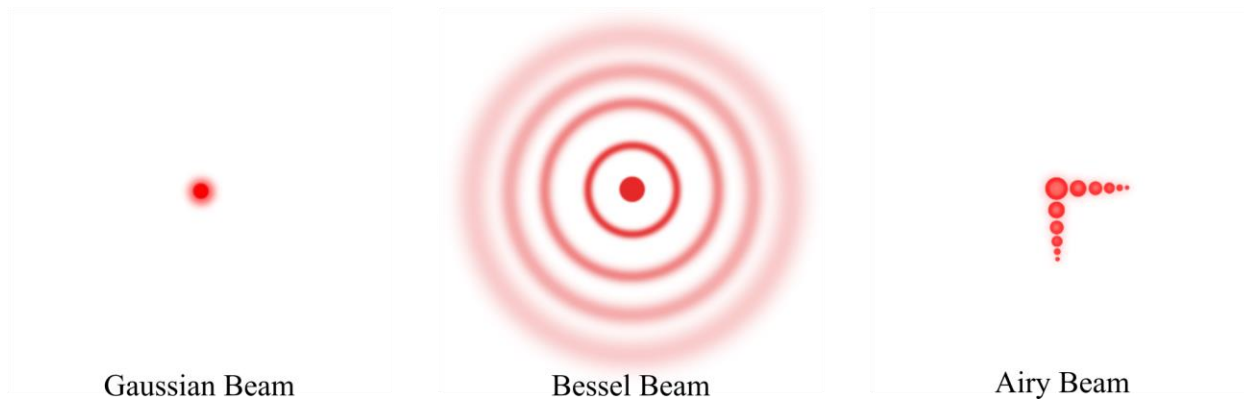


Figure 19: Types of Beams

In the Figure 19 we have representations of 3 types of beams. The first is gaussian which is a diffracting beam. Next is a Bessel beam, a non-diffracting beam. And 3rd is an Airy beam, another non diffracting beam. When a beam is described as non-diffracting, caution should be taken to not ascribe the non-diffracting behavior of the center lobe to the individual photons. This behavior corresponds to the center lobe of the beam, and only over a short distance, at the sacrifice of the outer beam features. In the case of the Bessel beam that would be the rings, in the case of the Airy beam, it would be the outer lobes.

The Bessel beam profile is like bullseye, a center dot surrounded by concentric rings. A true Bessel beam would have an infinite number of rings, never diffract and require infinite energy, therefore in the lab, for practical purposes, a truncated Bessel beam is used. Truncated Bessel beams have the property of self-healing, in which a blocking of the central lobe would provoke the concentric rings to recreate the center dot by sacrificing the rings, see Figure 20.

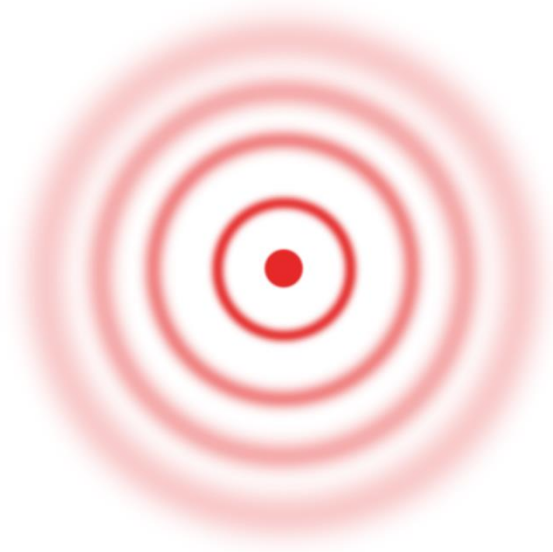


Figure 20: Bessel Beam

This happens via constructive interference of the expanding outer rings as the beam propagates.

The Airy beam profile has a center lobe, with in-plane side lobes extending away from the center lobe, with the side lobes perpendicular to each other meeting at the center lobe. A true Airy beam being infinitely non-diffractive, of infinite energy and infinite lobes cannot be produced in the lab, however a truncated version can be, and is better than the Bessel beam for penetration, healing, and additionally accelerating. See Figure 21.

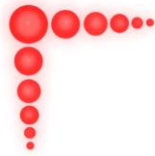


Figure 21: Airy Beam

In practice the limits to the non-diffraction aspects of these beams is the available power and aperture. However, even the limited non-diffraction length just has to be longer than the spatial features we require, at minimum $85\ \mu\text{m}$, ideally $100\ \mu\text{m}$ (Vettenberg 2014).

AIRY BEAM

Diffraction free (1+1)D Airy wave packets were predicted by Balazs and Berry in 1979. They showed via elementary quantum mechanics a non-trivial illustration of a non-diffracting wave with the ability to accelerate freely, even through empty space. Juxtaposing these waves to particles constrained to their momenta, and how what makes these waves behave as they do stems from the shape of the light itself. One of the assumptions was that Airy wave packet be of infinite energy, with tails or side lobes that were infinite as well. This is impractical and unachievable in the lab. Therefore, truncated diffractionless finite power Airy beams have been investigated by Siviloglou, when trying to characterize their propagation behavior. By beginning with the electric

field envelope and then describing the Airy function in the transverse direction, Siviloglou was able to show the Fourier spectrum of the beam in normalized k-space as:

14

$$\phi_0(\kappa) = \exp(-a\kappa^2) \exp\left(\frac{i}{3}(\kappa^3 - 3a^2\kappa - ia^3)\right). \text{ (Siviloglou 2007)}$$

Though 3 dimensional Airy wave packet “Bullets” can be created (Abdollahpour 2010), this work focusses on the 2 dimensional Airy beams created by this equation, representative beam is shown in Figure 22. How these types of beams are created will be discussed in another section.

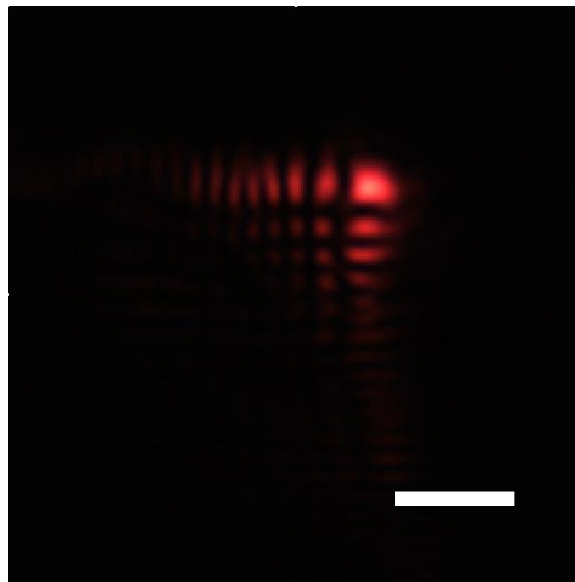


Figure 22: 2-D Airy Beam

OPTICAL FOURIER TRANSFORM

When the laser sends a pulse to the SLM, the SLM changes the phase front of the pulse. The phase front has the Airy function Fourier spectrum encoded in the transverse direction. When the pulse passes through a lens, the lens performs a Fourier transform on the incoming pulse. This is only valid with laser light. Any signal can be expressed as a sum of a series of sinusoids. Inside the input image we have spatial frequency that corresponds to the frequency of points across the

across space (here in the x direction). The magnitude in the input image corresponds to the brightness difference of the light and dark. And a phase corresponds to a shift in the transform. The take away message is that the inverse Fourier transform encoded on the SLM is Fourier transformed by the lenses. Thus if we know what we would like to produce after said lenses, we must first produce the inverse Fourier transform of it.

A microscope was built that takes the 3 concepts mentioned in the previous chapter (Airy Beams, Phase Masks, Optical Fourier Transform) and combines them in a way that allows for characterization and subsequent detection of any μm and sub- μm sized material that has a 2-photon response that can be flowed through a microchannel. At its most fundamental the airy beam at the focus point of the objective is a non-diffracting rod of light that is scanned to create a light sheet of uniform power and energy distribution. Particles that flow through said light sheet undergo 2-photon fluorescence that is then detected via a photo multiplier tube (pmt).

The microscope was built at the University of Texas El Paso Bio-Photonics lab in the physics department. The source laser is a femtosecond pulsed laser, Maitai HP, Spectra-Physics, 100 fs pulse length, tunable between 690 nm to 1100 nm, 2.5 W max power. The laser is guided to the flow cytometer table, and Spatial Light Modulator.

SPATIAL LIGHT MODULATOR (SLM)

The Holoeye PLUTO Spatial Light Modulator (SLM) has a Liquid Crystal on Silicon chip (LCOS) with approximate dimensions of 15mm x 9mm. The Mai-Tai laser has a width of ----- and must be expanded. The beam is passed through 2 converging lenses, with focal lengths 12.5cm and 20.0 cm, resulting in a beam that is 1.6 times its original width. This allows the laser to take full advantage of the SLM.

PLUTO SLM consists of a driver unit that accepts DVI or HDMI interfaces and a Liquid Crystal on Silicon chip (LCOS). It accepts a signal from a computer as an extended monitor device. The liquid crystal micro display is actually 1920 x 1080 pixel with each pixel being 8 μm . The electrical signal sent to the individual pixels changes the liquid crystal molecules such that their refractive index changes. Each of these changes affects the optical path length within that pixel. This allows for a phase change to be made to the wave front of each femtosecond beam pulse.

OPTICAL SETUP

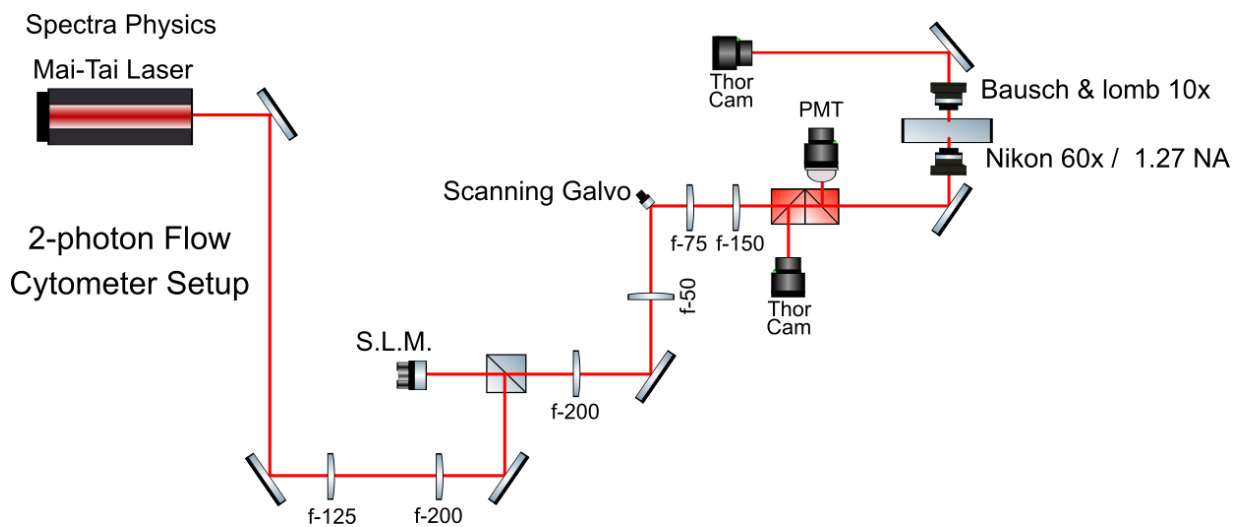


Figure 23: Optical setup of the Airy Beam Flow Cytometer

Figure 23 shows the optical setup of the Airy beam flow cytometer. The Mai Tai SP produces the femtosecond pulsed laser which is directed toward the flow cytometer setup. The beam must be expanded in order to optimize use of the entire SLM silicon chip. The SLM changes the phase of the laser before sending it forward through another pair of lenses that serve to reduce the size of the laser smaller than 7mm. The scanning galvo mirror is 7mm, and serves to deflect the laser some small angle. The angle is determined by the driving voltage, and is adjusted per experiment such that the laser is scanned 100 μm side to side. The laser must now be expanded via another pair of lenses that increases the laser diameter to fill the back aperture of the objective

lens. Before arriving at the objective lens, the laser passes through 2 dichroic mirrors that are angled to deflect fluorescence that follows the reverse path of the laser. The objective, a Nikon CFI Plan Apochromat VC 60XC NA 1.20, then focusses the beam on to the sample holder.

IN HOUSE PROGRAMS

In order for the SLM to affect the phase front of the laser pulses, the proper image must be displayed on the SLM, these are called phase masks. A code was written in python that produce phase masks by borrowing from Siviloglou et al. 2007. Siviloglou begins with the potential free Schrodinger equation. Then exploring a finite power Airy function as a solution to Schrodinger's equation. Of which the Fourier spectrum, in normalized k-space then leads to the transverse coordinates to be defined by equation 16. The code then plots this cubic function in x and y across a 2-dimensional image. In the images, black corresponds to the value 0 and white to the value pi. The results of the function displayed as gray valued pixels, are wrapped as if rastered, to create the mask that affects the wave front of the pulse via the SLM.

Airy mask production uses the Sivilglou 2007 function. Specifically, the phase portion of the equations. Where k_i is the transverse coordinate.

15

$$f_1 = \frac{k_i^3}{3} - k_i a^2$$

and in 2 dimensions

16

$$f = \left(\frac{k_x^3}{3} - k_x a^2 \right) + \left(\frac{k_y^3}{3} - k_y a^2 \right)$$

In order to replicate the article airy masks and have a -20π to 20π on the SLM, a total of $40\pi / 2\pi$ iterations of the modulo of the function must exist, this translates to 20 "wraps" of 2π .

Plotting the 1D case, then the function, then the "wrapped" function allows the user to see the number of "wraps".

Parameters that can be changed in the airy mask code are "width", "sampling", "a", and "dpi". Width is total span given to the transverse coordinate k , from -width to width (total 2width). Sampling is how many values must be taken between -width and width. DPI is the python plot parameter for dots per inch (affects resolution of final image, and consequently final size, this is vital for the SLM display). "a" is an equation weighting.

In order to reproduce the airy mask shown in the article the parameters were set to; Width = 3.6, Sampling = 800, a = 0.01, and DPI = 500.

The code displays work done as it progresses as a sanity check on airy mask production. Starting with; 1D mask, Full Function, Wrapped Function, Airy mask with sampling scale, and final Airy mask image. This displaying of the steps gives deeper intuition of the parameter effects. For example, changing the parameter "a" to 5.0 would change the weighting of the equation and change the "full function" graph from cubic toward linear, making the final mask unusable for the purposes of creating a non-diffracting airy beam.

Upon loading up the Airy phase mask images on the SLM computer in the lab it was discovered that the images had a "frame" of transparent white. This translated to a repeated white bar on the SLM driver software from HoloEye. Inside the python coding the "plt.savefig" function that saves the created figure adds this as padding. Setting the padding to zero did not help. Only after some experimenting was it discovered that setting the "pad inches" parameter to -0.01 inches made the padding disappear.

Images on the screen also suffered from being too large. HoloEye Screen resolution is

1680x1050. Python images are 1855x1855. In order to accommodate the HoloEye resolution, the appropriate resolution is “cut out” from the python images. Both the original image and the correct resolution image are then saved to the root directory.

For code see: Appendix B: Python Code for Airy Mask Production.

PHASE MASKS

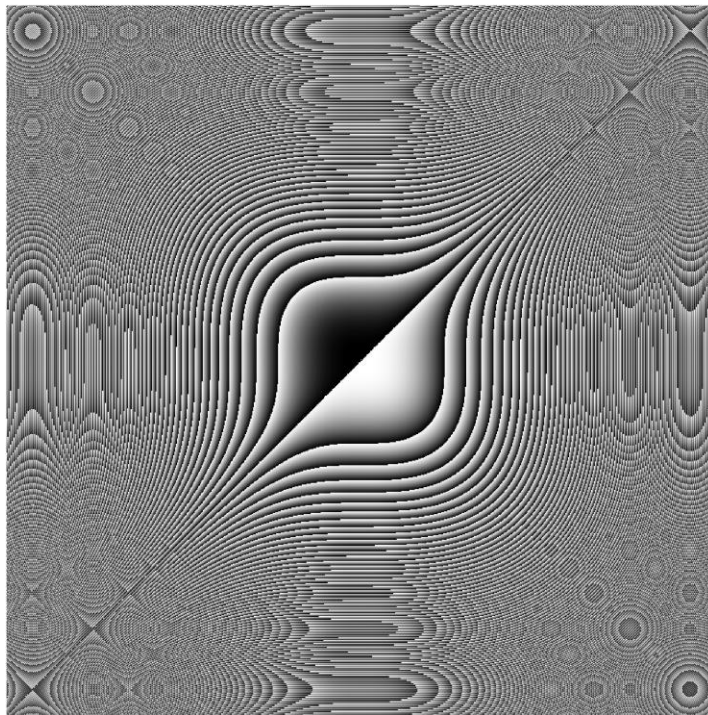


Figure 24: Example of the Airy Mask

Here we see examples of the Airy masks that were produced, Figure 24 These are not the appropriate resolution for use on the SLM. These are trimmed for presentation purposes. The appropriate phase masks must match the SLM resolution of 1920 x 1080 pixels and be centered for the SLM software. The Holoeye software opens the image correctly, centered, and offers adjustment tools within the application to affect things like spherical aberration which is a software equivalent to placing a lens in contact with the SLM of different focal lengths. For example,

spherical aberration -16 is equivalent to placing a lens of focal length of 10.61 meters. This helps to ultimately fine tune the projection of the phase mask onto the SLM which in turn affects the wave front of the beam. The maximum phase retardation on the SLM is 2.6π for 710nm.

Once the beam leaves the SLM, it continues toward a scanning galvo mirror, or galvo for short. The Galvo, is a small motor connected to a small mirror. The motor vibrates at a defined frequency, making the mirror vibrate, thus scanning the beam in the x axis. The galvo mirror is 6mm by 7mm. This requires that the beam be narrowed prior to arriving at the galvo. The beam is passed through 2 converging lenses, with focal lengths 200 mm and 50 mm, resulting in the beam reducing to 3mm diameter. The galvo can scan up to 20 degrees of optical deflection, and/or up to 50,000 pulses per second. These parameters are controlled independently via a signal generator connected to the galvo inputs. The signal generator frequency corresponds to the galvo mirror's scanning frequency, and the voltage sent by the signal generator corresponds to the amplitude of the scan or how wide the scan should be. This allows for precise control of scanning rate and scanning distance for fitting of the laser beam into an $85 \times 85 \mu\text{m}$ area at the target.

Scanning parameters are defined per experiment. The eventual purpose of the flow cytometer is to probe blood flow in mice for indicator cells. Blood flow velocities in the thinnest of blood vessels, the capillaries and venules, is about 2 mm/s (Unekawa; et al. 2010). This translates to $2000 \mu\text{m} / \text{sec}$. Setting the microfluidic channel flow velocity accordingly, means that a flowing blood cell $7 \mu\text{m}$ across would cross any random point in $3.5 \text{ E-}3$ seconds. This sets our scanning frequency minimum at 285 Hz. Frequency maximum is computed by taking the lifetime of a point passing through the $3 \mu\text{m}$ thick light sheet. A point will take $1.5 \text{ E-}3$ seconds to cross the light sheet. Therefore, frequencies above 666 Hz should only be used if double sampling of a

7 μm cell is required. Experimentally, we would keep the frequency at 444 Hz in order to avoid aliasing of signals (Oomen; et al. 2007).

During two-photon fluorescence, two-photon absorption velocity is in the femtosecond range. The electron then has a vibrational relaxation time reported to be in the nanosecond to femtosecond regime before falling to the ground state (Bott 1972).

The scanned beam is then guided toward the objective. The laser beam must be expanded to optimize the use of the objective lens. 2 converging lenses of focal lengths 75 mm and 150 mm are used resulting in an expanded beam. The expanded beam passes through a beam splitter that sends remainder signal to a Thor Camera used for real time observations, then a 630 nm dichroic mirror before the objective lens that sends fluorescence signal below 630 nm to a photo multiplier tube. Beyond the dichroic is an objective lens which serves to focus the laser on the sample area.

A Nikon CFI Plan Apochromat VC 60XC NA 1.20 objective lens with a working distance of 250 μm was installed. This objective focuses the laser on our target while simultaneously capturing fluorescence. Depending on what is being displayed on the SLM the laser can focus to a gaussian beam, or a nondiffracting airy beam. In either case the laser is being scanned at 444 Hz. Scanning the laser creates a scanned gaussian beam, which is functionally a line of laser at the gaussian focus. In the case of the non-diffracting airy beam, a light sheet is created whose dimension is contingent on the optimization of the Airy beam. The depth of the sheet is the size of the Airy beam central lobe, approximately 3 μm . The width is controlled by the galvo and is approximately 100 μm . The length of the Airy light sheet is determined by the non-diffraction propagation length of the particular Airy beam being used, it is on the order of 100 μm . Thus the Airy light sheet would be approximately 3 x 100 x 100 μm if at the gaussian focus, contingent on individual Airy beam characteristics.

Z-LOCATION OF, AND CO-LOCATING THE MICROCHANNEL AND AIRY SHEET

The flow cytometer must replicate the flow of blood in a mouse blood vessel. Detection of a fluorescent signal is contingent on the airy sheet being co-located on the simulated blood vessel. This blood vessel is simulated by a microfluidic chip from the Microfluidic Chip Shop. The polymer chip has a microchannel cut into the polymer. The micro channel inside the chip is 85x85 μm and is located 80 μm below the surface of the chip (this places the microchannel within the working distance of the Nikon 60x 1.2NA objective). The microchannel traverses the length of the chip and terminates with Luer Lock quick adapters for using microbore syringes and tubing. In the optical setup, Thor Camera 2 allows for real-time visual feedback to locate the microchannel in X and Y. The Z location of the channel is more difficult to attain.

The microfluidic channel is mounted on a 3 axis translational stage. During operation a syringe pump will flow microbeads or cells in appropriate solutions, through the syringe, tubing, and microchannel at velocities that are defined per experiment. The purpose is to mimic the flow of blood of a mouse capillary, at 2000 μm /second. Some problems may be encountered with thicker coverslips, and/or slides and appropriate steps should be taken to ensure all test slides fall within the short working distance of the objective lens.

During an experiment a fluorescent bead or cell will flow through the microchannel and as they pass the objective lens, the flow intersects with the airy light sheet. This light sheet must be created in such a way, that it covers the entire cross-sectional area of the microchannel, so that a particle that flows through the light sheet can then undergo 2-photon fluorescence. This requires a characterization of the Airy light sheet. In order to characterize the Airy light sheet, first, intensity profiles of many Airy beams were plotted with respect to the gaussian focus. Airy beams were varied using different airy masks with adjusted modulation, spherical aberration, and fine tuning

of the SLM location. Intensities of the airy beams were taken every 25 μm , for 250 μm , centered at the gaussian focus, then plotted together, Figure 25.

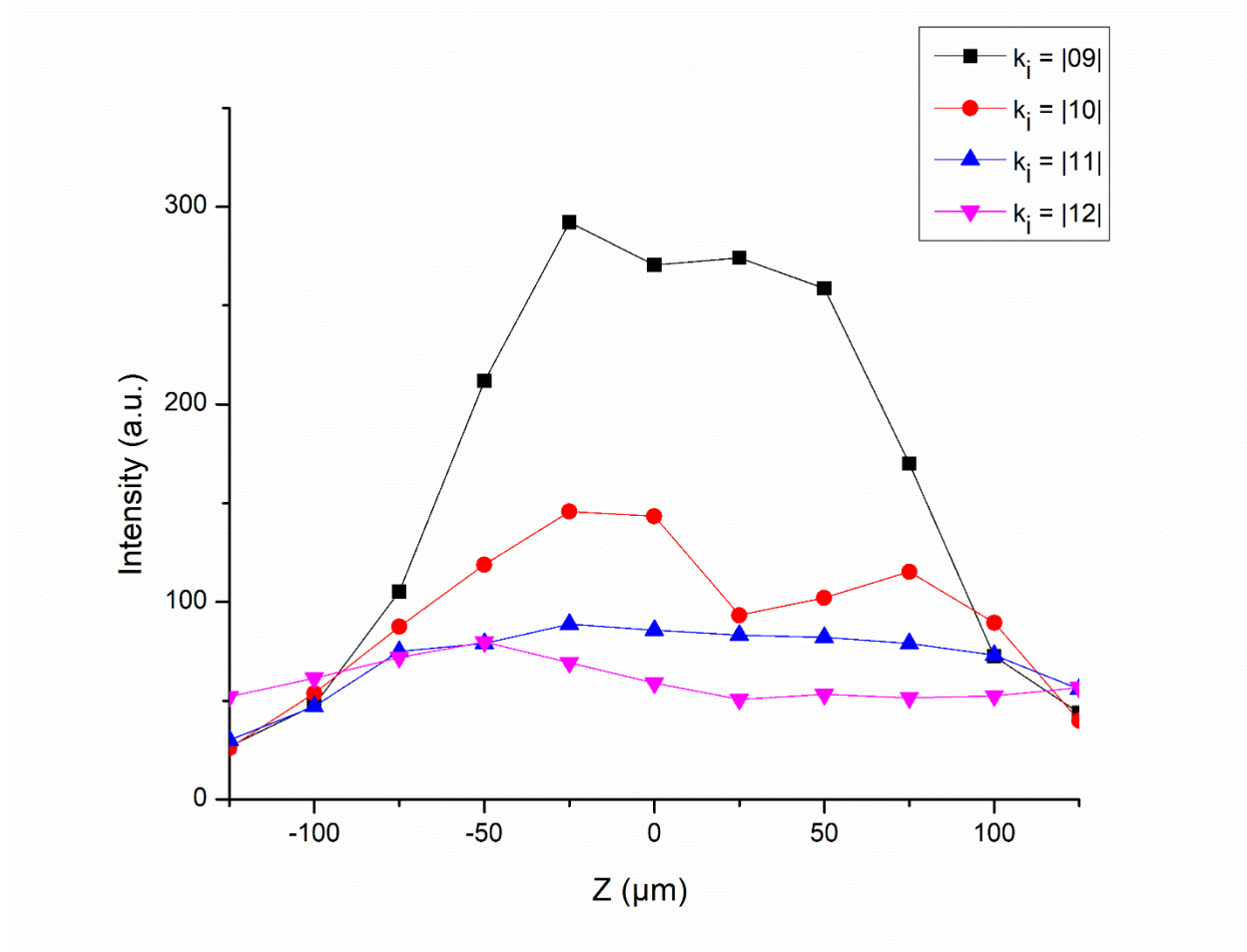


Figure 25: Intensity of the Airy Beams Plot

As shown in Figure 25 airy beam 9 with aberration negative 16 produced the appropriate length and extends beyond the gaussian focus both in the positive and negative directions. If the gaussian focus is placed at the center of the microchannel in the Z direction, when the SLM is switched on to change the gaussian beam into an airy beam, the airy beam is in the correct placement for the light sheet to overlap the microchannel.

The second Thor Camera allows for real-time visual feedback to locate the microchannel in X and Y. The Z location of the channel is more difficult to attain. It has been shown how the

gaussian focus corresponds to the airy beam intensity profile. This tells us that the location of the gaussian focus maps to a point on the light sheet that is close to the center of the light sheet. The microchannel has 3 surfaces that will reflect light back through the objective. As the light returns from the reflective surface, it is directed through a dichroic mirror that transmits wavelengths greater than 605 nm. The fluorescence signal is expected to be around 525 nm, and the laser wavelength is 710 nm. Any reflected light that is not due to fluorescence should pass through the dichroic and be diverted into the Thor Camera 2 via a beam splitter.

The first surface of the microfluidic chip that should reflect light is the top of the cover, next is the back surface of the cover which happens to be the top surface of the microchannel, and last is the back surface of the microchannel. If the SLM is set to gaussian beam, and the objective is lowered, it creates a line-scanned-gaussian that will reflect from surfaces. When the first surface of the microchannel intersects the line-scanned-gaussian, a pattern appears on the Thor Camera 2 video feed. If the microchannel chip surface is perfectly parallel with the scanned gaussian, the pattern appears as a uniform line across the microchannel surface. If the rod of light is not uniform, then the microchannel must be rotated along the X or y axis to make the rod uniform. Continuing to lower the objective, the rod of light then reflects off the top surface of the microchannel. The width of the line-scanned-gaussian can be fine-tuned to be precisely 100 μm by using the microchannel as our scale and making the line-scanned-gaussian 15 μm bigger than the microchannel and evenly distributed on either side of the channel. Lowering the objective further, the last surface to reflect the line-scanned-gaussian is the back surface of the microchannel. By noting the stage locations for the top and bottom surfaces of the microchannel we can center the line-scanned-gaussian. Once the SLM is switched to airy mode, the light sheet created will be co-located on the microchannel.

DETECTION AND DATA CAPTURE OF FLUORESCENCE SIGNAL

The airy beam light sheet is sufficiently intense to provoke 2 photon fluorescence in microbeads or tagged cells that flow through it. The energy of the photons emitted due to the 2 photon fluorescence must be less than twice the energy of the laser photons. In this case, the emitted photons would have a wavelength of around 525 nm. Reflected 710 nm, and fluorescence 525 nm photons, return thorough the objective lens, and then diverge at the 605 nm dichroic mirror. The dichroic allows the 710 nm photons to continue toward Thor Camera 2. However, it reflects all photons of wavelength less than 605 nm to the PMT. The PMT takes particle counts and sends an analog signal to the National Instruments Externally Powered USB Data Acquisition Device (DAQ).

The PMT is connected to a power supply, and to the DAQ. The Power supply provides the driving voltage for the PMT internals. A single photon arrives at the window on the PMT. The PMT design is such that the impinging photon on a metal plate, releases electrons due to the photo electric effect. These electrons are released toward a secondary plate that multiplies the number of electrons moving through the PMT. This process continues, the cascade of electrons falling toward a final anode held at a potential. The driving voltage can cause the PMT to cascade a higher number of electrons, thus multiplying the original signal. This is ideal for low intensity signal detection. Care must be taken to not use a driving voltage that is too high. This can cause un-wanted noise in the detected signal, or can burn out the PMT. The analog signal is sent via coaxial cable with BNC connectors to the DAQ.

The PMT analog signal is not appropriate for direct connection to a computer, therefore it is sent through the DAQ. The DAQ is a waypoint for the data between the detector and the computer's software. The DAQ can sample the analog signal and capture the data as a time series.

The NI DAQ 6341 must be warmed up for 15 minutes for all circuits to stabilize. It can take up to 500,000 samples per second in one channel. Or appropriately distributed among 2-10 channels, for example 250,000 samples per second each, through 2 channels. For the purposes of the flow cytometer, only one channel is required. Once connected to the computers COM port, a code in an appropriate language can call on the DAQ's functionality.

The flow cytometer uses a custom python code. This python code sends a signal to the DAQ to begin data acquisition for some amount of time, at some number of samples per second, and various other parameters. The DAQ begins to fill its internal buffer, then dumps to the computer's RAM. The data takes the form of analog voltages sent as a time series defined by samples per second taken. Once the experiment's time-to-run is over, the DAQ stops collecting data, and the python code then takes the data on the computer's ram and saves it to the hard disk as a .csv file. Data collection at 250,000 samples per second and collecting for 180 seconds creates a 1 gigabyte file. This puts a cap on the amount of data that can be collected per run. The computer has 16 gigabytes of ram, of which 8 is available normally. This means that our theoretical maximum single run data collection is limited to the order of 24 minutes. However, when tested in the lab, this was found to be false. The computer's performance allowed for a real maximum time per run of 10 minutes. Running data capture for 10 minutes would occasionally cause stability issues that appear to be arbitrary or tied to background processes in the operating system. This can be circumvented by running multiple experiments of less time. It was found that both from a data collection and data processing point of view, optimal time-to-run was 60-second experiments.

The python code must import the National Instruments library along with numpy, and matplotlib. The logic flow of the code is as follows;

1. Define Samples per second

2. Define how many samples to take total
3. Setup an array of zeros with length equal to total samples
4. Call the nidaqmx task and define the following parameters
 - a. Channel to capture: Dev2/ai0
 - b. Timing set to: Samples per sec, Rising Edge, Acq=Finite, total samples
 - c. Taks.read set to: total samples, and “WAIT_INFINITELY”
5. Use numpy to save text file as a CSV defining the delimiter as a comma

Python code for data capture is in Appendix C: Python Code for Data Capture.

The data captured by the flow cytometer is a time series of voltages sampled directly from the PMT by the DAQ. Consider that at 250,000 samples per second, for 60 seconds, produces a 0.385 gigabyte and that a typical run captures 60 minutes of data, this means that the research must scour through 20 gigabytes of data per run. For this purpose, a python code was written to process the data.

The python signal processing and peak finding code runs on a separate computer that is not part of the flow cytometer. This is done to be able to parallel process while data is being captured. There is the characteristic background floor for the PMT, and then high intensity signal peaks. As

shown in Figure 26 of a trace while scanning over a microbead.

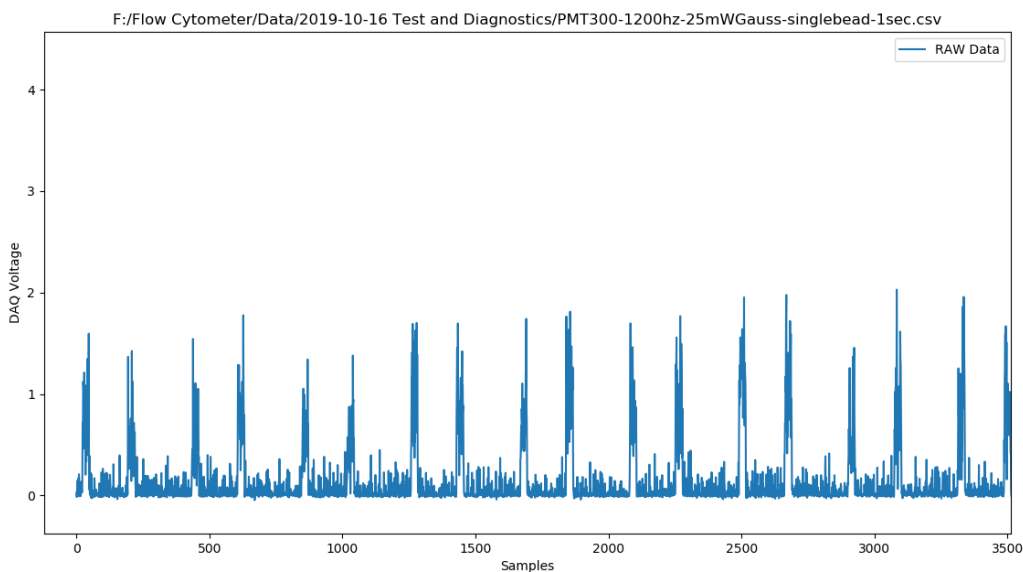


Figure 26: Test and Diagnostics PMT300-1200hz-25mWGauss-single bead-1sec

The raw background signal from the PMT has a high frequency background with occasional spikes that are considered noise. In order to extract signals from the raw data, the code performs a sliding window average across 10 samples creating a new array of data. This new smoothed data is then passed through the peak finding algorithms in order to get counts. The peak finding algorithm must be defined via parameters that tell the code the expected fluorescence response peak widths, peak minimum height, peak repeatability, and peak distance. These must be adjusted on a per experiment basis.

Python code for signal processing and peak finding is in

Appendix A: Python Code for Peak Finding.

OPTIMIZATIONS OF THE FLOW CYTOMETER

Great care is taken to build the optics and electronics for the flow cytometer. However, there are smaller details that only become apparent during full scale operation, that can be optimized. A working knowledge of the flow cytometer is required before we address them. That is why this section is placed here.

During full scale operation it was noticed that the noise level of the PMT would change when another component, the galvo mirror, would start, stop, or change its frequency. The change was small but offered a clue to pursue during the optimization period. Both the PMT and galvo mirror wires, controllers, voltage regulators, and accessory components were electrically isolated from each other and the optics table. The PMT high voltage wires were shielded and arranged in order to minimize coupling. A trace was taken showing that isolating the PMT would cause a drop in noise as shown in Figure 27. As a precaution additional grounding was added to all optics tables, equipment stacks, and components.

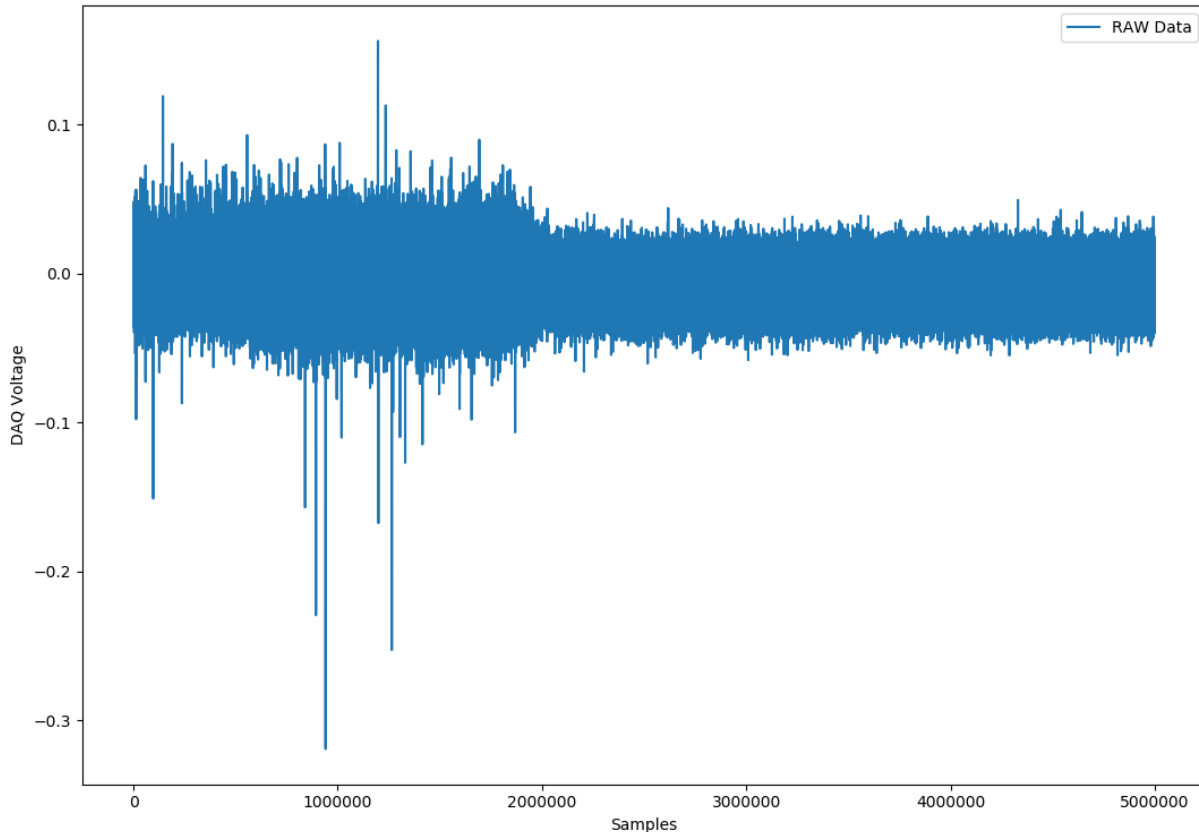


Figure 27: Trace showing DAQ noise drop by isolating the PMT. At 2000000 samples the PMT was removed from the Optics table and placed on an electrical insulator.

Dark traces were taken to characterize the PMT noise, post electrical isolation and grounding. It was found that the PMT produced spikes of voltage up to 6 times higher than the noise floor, that were lasting 2 microseconds, or one sample by the DAQ. Because of this the DAQ was isolated and checked by shorting the negative and positive connections of the BNC connector at the analog input Dev2/ai0. This produced a characteristic grounded signal that is used in the calibration process, effectively eliminating the DAQ as the source of this one sample noise peak. Literature searches on the Hamamatsu R10699 PMT revealed that this type of noise could be reduced by cooling the PMT to -30° Celsius (Hamamatsu, 2007). A box was formed around the PMT, made from corrugated plastic, cold weather adhesives, and cold weather aluminum tape. The empty space was then filled with a black flannel cloth material to create a separation barrier

between the PMT housing and the cooling method. Dry ice was used to cool the cooler box and keep the PMT cold. This significantly reduced the number of spike noise as shown in Figure 28.

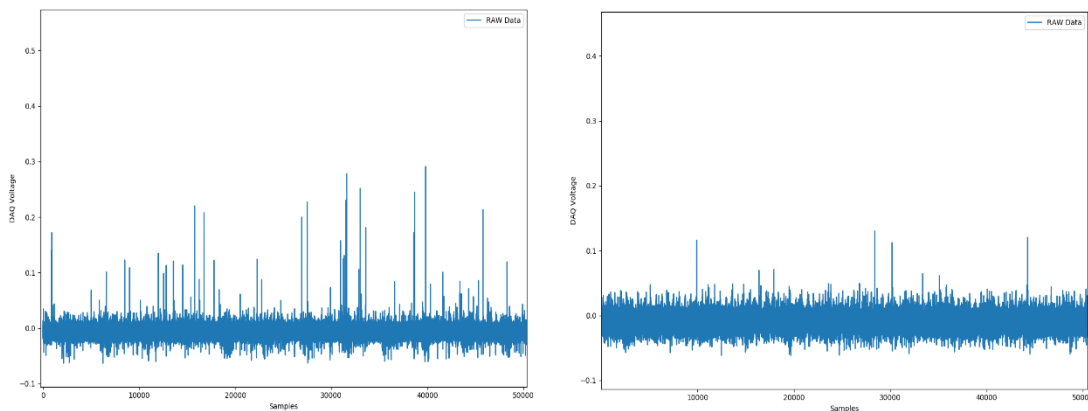


Figure 28: Data without and with Dry ice

Once the cells had been received, and appropriate characterization of the cells was performed, it was seen that the cells were fluorescing at 920 nm light, thus requiring a complete re-optimization of the flow cytometer away from 710nm. The flow cytometer is built sufficiently robust that a change of this nature can be done in less than 6 hours. Optimization for a new wavelength requires the following parameters and situations be addressed.

First, the flow cytometer must be shifted into “characterization mode”, this means that the dark box that keeps stray light out of the flow cytometer must be removed, and the beam characterization stack (the stack is a piece of optical track that is mounted vertically in such a way that it can fold the light beam backward and above the optics table toward a characterization camera) must be rotated into place. Then the Mai Tai is tuned to the new wavelength, in this case 920 nm, and warmed up. With all the computers on, and no scanning on the galvo an image can be captured by the characterization Thor cam. Adjustments need to be made first to the physical SLM 3d adjustable stage mounts, while simultaneously verifying the quality of the beam on the Thor cam video feed. Movement of the SLM in the x direction (transverse) causes a change in the x direction sidelobes of the Airy beam. Similarly, it should be done with the y direction. Adjusting these two gives the “best” quality beam, where the side lobes are even and set orthogonal to each

other. Only after this should the aberration of the Holoeye software be adjusted. The same protocol should be used to find the “best” propagation length of the new Airy beams, and the characterization of the gaussian focus, versus the Airy beam propagation. The combination of all of these should create a repeatable “map” for the co-location of the scanned Airy beam light sheet and the microfluidic channel. In the case of the 920 nm excitation light, it was found that Airy beam 06 with an aberration of zero created the ideal light sheet.

RESULTS

The non-linear airy beam flow cytometer has shown that use of a scanned airy beam creates a light sheet of significant intensity across a microchannel. Also, that it can stimulate 2-photon fluorescence from fluorescent microbeads and tagged cells while flowing. By controlling scanning rates and careful video capture, peak counting by the python code could be verified.

A sample of 15 micron microbeads in a solution made of 1% Polysorbate 80, 99% distilled water by volume was created with a concentration of 100,000 beads per ml. At a flow rate of 0.0006 ml / minute, it is expected that there would approximately be 1 microbead per second flowing through the airy light sheet. Simultaneous video of microchannel was taken for visual counting of the beads. A typical trace of the peak finding is shown in Figure 29.

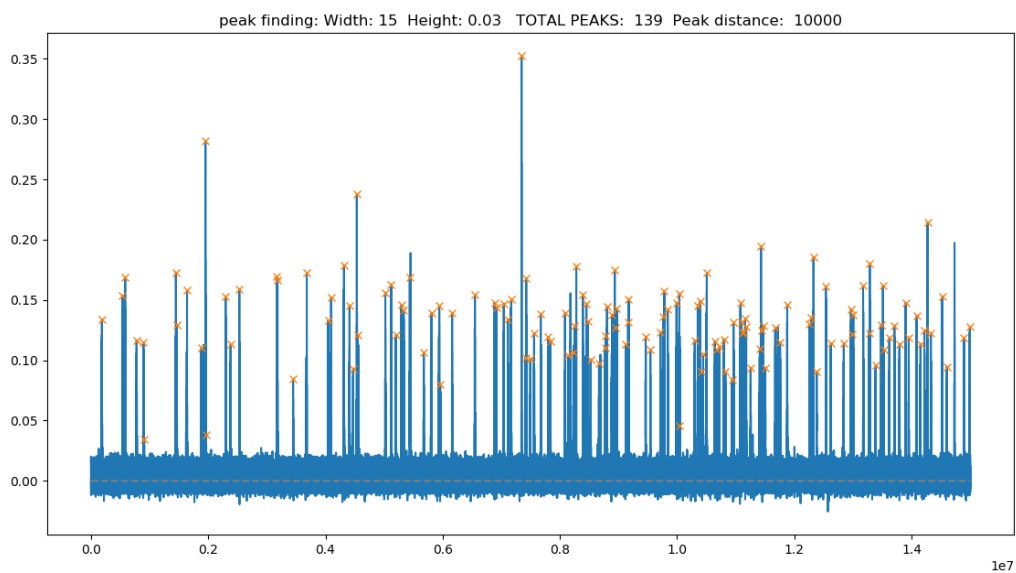


Figure 29: Results.

Video was processed frame by frame and counts taken for each bead that crossed the airy light sheet threshold. Time series data was processed through the peak finding code, and comparison made to the video count. This is represented in Figure 31.

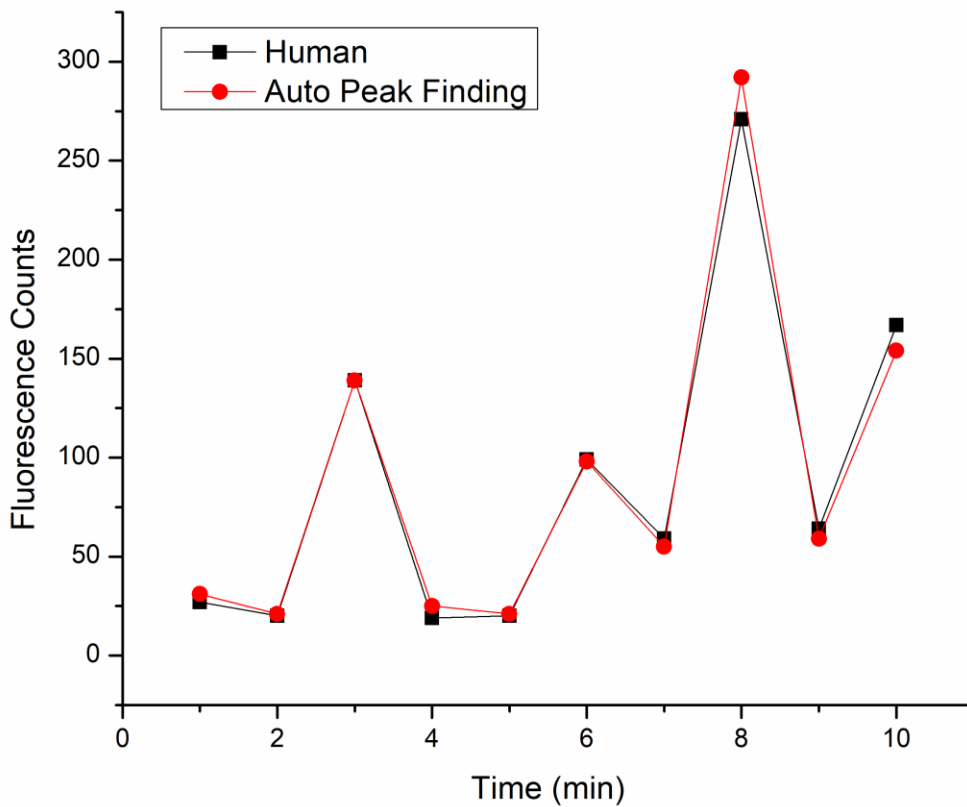


Figure 31: Verification of Auto-counting Mechanism against human count

On average the counts were within 9% of each other. Careful analysis of the discrepancies found that the peak finding code would not count beads that were behind one another in line with the laser propagation direction, however the human counter could distinguish the double bead on video. It was also found that the peak finding code was counting beads that were crossing the laser light sheet threshold between the frames of the video, in these cases analysis of the frames prior and post detection show a bead entering frame and exiting frame, thus it must have crossed the laser light sheet. This validates the flow cytometer for counting flowing fluorescent particles 15 μm across.

Biological samples were also counted. At the time of this writing the fluorescence tagging was far too weak as shown in Figure 30. Image was taken with the 2-photon microscope at 100mW. This will not fluoresce under the flow cytometer. New samples are being grown that should be more fluorescent and of greater number.

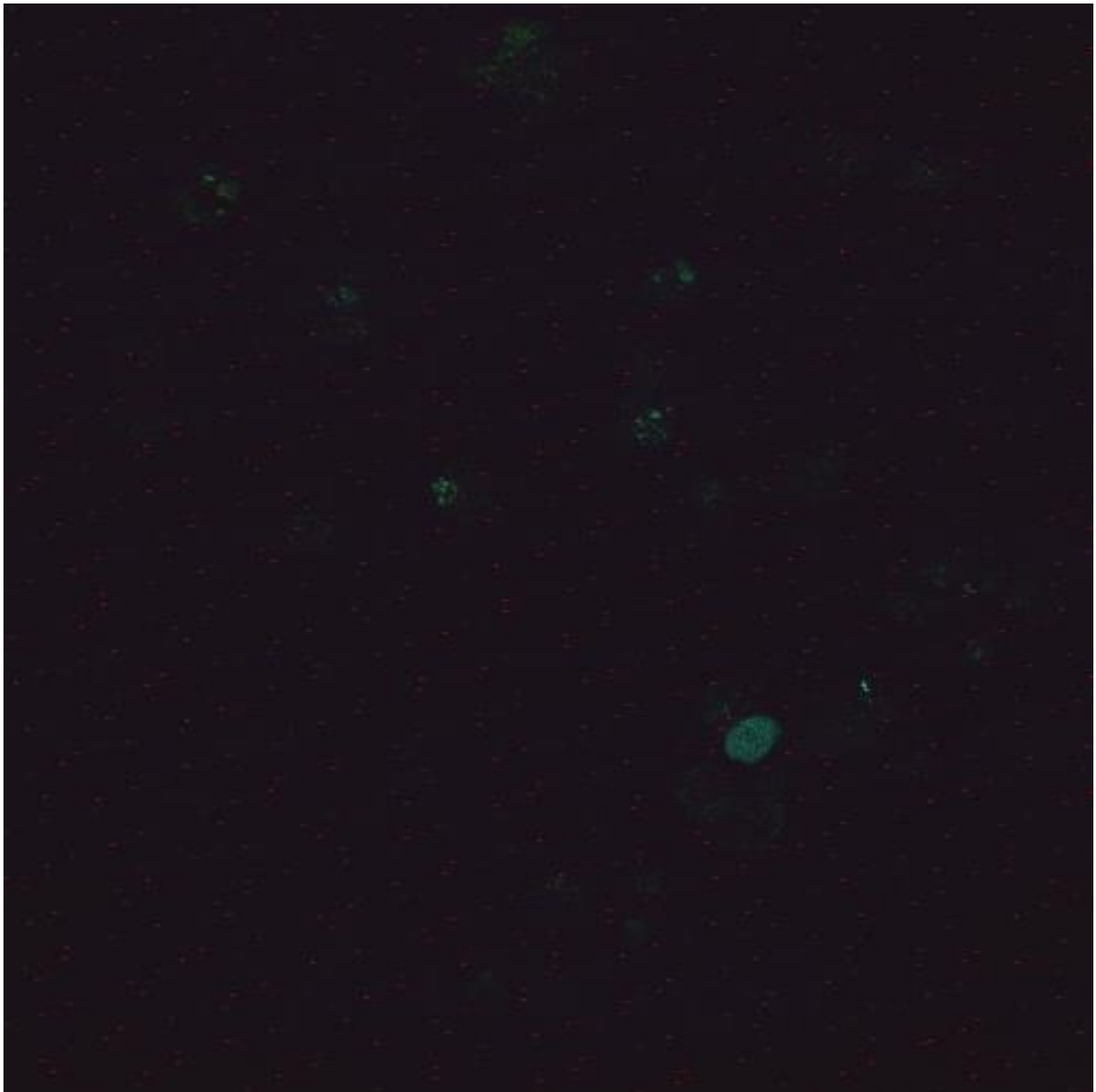


Figure 30: Fluoresce Tagging in a Biological Sample

The cells were from the WI-26 cell line, a human diploid fibroblast cell line from embryonic lung tissue. These cells were tagged with pcDNA3.1-GFP

FUTURE WORK

To further validate the flow cytometer, another experiment was designed, using 1 μm fluorescent beads that were flowed through the flow cytometer at various flow speeds. This experiment shows that the flow cytometer will detect fast moving, μm sized particles, and validate the sensitivity of the instrument given short lifetime fluorescence. This experiment as well as the tagged cells and in-vivo cases are left as future work for the photonics lab.

References

- Abdollahpour, Daryoush. "Spatiotemporal Airy Light Bullets in the linear and nonlinear Regimes." *Physical Review Letters*, December 2010.
- Akter, F. *Tissue Engineering Made Easy*. Academic Press, 2016.
- Bott. "HF Vibrational Relaxation Measurements Using the Combined Shock Tube Laser induced Fluorescence Technique, Vol 57 number 1]." *The Journal of Chemical Physics* 57, no. 1 (1972).
- Givan, Alice L. "Flow Cytometry: An Introduction." In *Flow Cytometry Protocols, Methods in Molecular Biology*, by Teresa S. Hawley, & Robert G. Hawley, 1-29. Humana Press, 2010.
- Goeppert-Mayer, Maria; Göttinger. "Disertation Reprint of "Über Elementarakte mit zwei Quantensprüngen"." *Annalen der Physik* 9[401] (Annalen der Physik 9[401]), 1931: 273-294.
- Hamamatsu Photonics; "Photomultiplier Tubes, Basics and Applications, Third Edition (3A), Photon is Our Business."; Hamamatsu Photonics K. K.; 2007
- Hatch, K.A.; Ornelas, A.; Williams K. N.; Boland, K.; Michael, K.; Li, C. "Photolysis of a peptide with N-peptidyl-7-nitroindoline units using two-photon absorption." *Biomed. Opt. Express* 7 (2016): 4654-4659.
- Horton, N.G; et al. "In vivo three-photon microscopy of subcortical structures within an intact mouse brain." *Nat Photon* 7, no. 3 (2013): 205-209.
- Kaiser, W. "Two-photon excitation in CaF₂Eu²⁺." *Physical Review Letters* 7, no. 6 (September 1961).
- Kong, L.; Tang, J.; Cui, M. "Multicolor multiphoton in vivo imaging flow cytometry." *Optics Express* 24, no. 6 (2016): 6126-6135.
- Lakowicz, Josph R. *Principles of Fluorescence Spectroscopy*. Kluwer Academic / Plenum Publishers, 1999.
- Laschke, M.W.; Menger, M.D.; "Vascularization in tissue engineering: angiogenesis versus inosculation." *Eur. Surg. Res* 48 (2012): 85-92.
- Obrien, F. "Biomaterials & Scaffolds for Tissue Engineering." *Material Today* 14, no. 3 (March 2011): 88-95.
- Oomen; et al. "Aliasing of Resonance Phenomena in Sampled Data Feedback Control Design: Hazards, Modeling, and a solution." *American Control Conference*. New York City: IEEE, 2007.
- Ornelas, A.; Paez, A. "Synthesis and characterization of a photocleavable collagen-like peptide." *Organic & Biomolecular Chemistry*, January 2018.
- Pons, Thomas. "In Vivo Imaging of Single Tumor Cells in Fast-Flowing Bloodstream Using Near-Infrared Quantum Dots and Time-Gated Imaging." *ACS Nano* 13, no. 3 (2019): 3125-3131.
- Roberts, B.C.; "NASA SLS-SPEC-159 Cross-Program Design Specification for Natural Environments (DSNE) Revision E"; 2017
- Rulliere, Claude. *Femtosecond Laser Pulses, Principles and Experiments*. 2nd. New York: Springer Science, 2005.
- Siviloglou, Georgios A. "Accelerating finite energy Airy Beams." *Optical Society of America*, March 2007.

- Tan, Xufei. "In Vivo Flow Cytometry of Extremely Rare Circulating Cells." *Scientific Reports* 9 (March 2019).
- Unekawa; et al. "RBC velocities in single capillaries of mouse and rat brains are the same, despite 10-fold difference in body size." *Brain Res*, 2010: 69-73.
- Utzinger, U.; Baggett, B.; Weiss, J.A.; Hoying, J.B.; Edgar, L.T. "Large-scale time series microscopy of neovessel growth during angiogenesis." *Angiogenesis* 18 (2015): 219-232.
- Vettenberg, Tom. "Light Sheet microscopy using an Airy beam." *Nature Methods*, no. 11 (April 2014): 541-544.
- Xu, Chris. "Measurement of two-photon excitation cross sections of molecular fluorophores with data from 690 to 1050 nm." *Journal Optical Society of America*, Vol 13, No. 3, (March 1996): 481-491.

Appendix A: Python Code for Peak Finding

```
-----Begin Code-----

import matplotlib.pyplot as plt

import numpy as np

from numpy import cos, sin, exp, pi, arccos, tan, sqrt, arctan, arcsin, arctan2

import tkinter as tk

from tkinter import filedialog

import scipy

from scipy.fftpack import fft, ifft

from scipy.signal import savgol_filter

from scipy.signal import find_peaks, peak_widths

file_path = filedialog.askopenfilename(filetypes=[("all files", "*..*")])

print("plotting csv file")

#####

###Plotting of CSV file

y = np.loadtxt(file_path, delimiter=',', unpack=True)

y = [float(i) for i in y]

n = len(y)

x = np.linspace(0, n, num=n)

plt.plot(x,y, label='RAW Data')

plt.autoscale(enable=True, axis='both', tight=None)

plt.xlabel('Samples')

plt.ylabel('DAQ Voltage')
```

```

plt.title(file_path)
plt.legend()
plt.show()

#####

#####

def moving_average(a, n=10) :
    ret = np.cumsum(a, dtype=float)
    ret[n:] = ret[n:] - ret[:-n]
    return ret[n - 1:] / n

ymov = moving_average(y)

n = len(ymov)
x = np.linspace(0, n, num=n)

SMALL_SIZE = 15
MEDIUM_SIZE = 15
BIGGER_SIZE = 15
PRINT_SIZE = 66

plt.rc('font', size=SMALL_SIZE)
plt.rc('axes', titlesize=MEDIUM_SIZE)
plt.rc('axes', labelsiz=MEDIUM_SIZE)
plt.rc('xtick', labelsiz=SMALL_SIZE)
plt.rc('ytick', labelsiz=SMALL_SIZE)
plt.rc('legend', fontsize=SMALL_SIZE)
plt.rc('figure', titlesize=BIGGER_SIZE)

plt.plot(x,ymov, label='_nolegend_')

```

```

plt.autoscale(enable=True, axis='both', tight=None)
plt.xlabel('Samples')
plt.ylabel('Voltage (V)')
plt.legend()
plt.show()

#####

print("finding peaks")

height = 0.03
distance = 10000
width = 15

peaks, _ = find_peaks(y mov, height=height, distance=distance, width=width)
numpeaks = len(peaks)

plt.plot(y mov)
plt.plot(peaks, y mov[peaks], "x")
plt.plot(np.zeros_like(y mov), "--", color="gray")
plt.show()
print ("done")

```

----End Code----

Appendix B: Python Code for Airy Mask Production

```
***Begin-Code***

import matplotlib.pyplot as plt

import numpy as np

import math

from math import e

from PIL import Image

#####

# Variables that can change

width = 15          #width of sampling space k and y

sampling = 3200     #defines number of samples in width

a = 0.01           #Truncating Factor must be <<1

dpi = 520          #scalar value >0 dots per inch (resolution control)

#####

k = np.linspace( -width, width, sampling)

y = np.linspace( -width, width, sampling)

f = ((k**3)/3)-(k*a**2) +((y**3)/3)-(y*a**2)

print (f)

print ("ok")

print ("width = ", width)

print ("sampling =", sampling)

print ("a = ", a)

print ("dpi = ", dpi)

z = (f % np.pi)

#np.savetxt('testy.txt', f)

#np.savetxt('testx.txt', k)

#np.savetxt('testz.txt', z)
```

```

plt.imshow(z,z), extent=[-width, width, -width, width], cmap='binary', aspect=None,
vmin= 0, vmax= 3.14)

plt.title('1D Airy Mask (positive & negative)')

plt.show()

#####

plt.plot(f)

plt.xlabel('SAMPLING of wave number (k)')

plt.ylabel('(1/3 k^3)-(k a^2)')

plt.show()

#####

plt.plot(k, z)

plt.xlabel('wave number (k)')

plt.ylabel('(1/3 k^3)-(k a^2) modulo 2pi')

plt.show()

#####

X,Y = np.meshgrid(y, k) # Create 2-D grid xlist,ylist values

Z = (((X**3)/3)-(X*a**2) +((Y**3)/3)-(Y*a**2)) % 2*np.pi # Compute function values on
the grid

#plt.contour(X, Y, Z, colors = 'gray', linestyle='solid' ) # [0.5, 1.0, 1.2, 1.5]

#plt.show()

#np.savetxt('testZZZ.txt', Z)

#####

plt.imshow(Z, cmap='binary', vmin= 0, vmax= 3.14)

plt.show()

#####

fig = plt.imshow(Z, cmap='binary', vmin= 0, vmax= 3.14)

plt.axis('off')

fig.axes.get_xaxis().set_visible(False)

```

```
fig.axes.get_yaxis().set_visible(False)

plt.savefig('pict.png', orientation='landscape', bbox_inches='tight', pad_inches = -
.01, dpi = 520, frameon = None)

plt.show()

#####

i = Image.open('pict.png')
frame2 = i.crop(((0, 420, 1917, 1500)))
frame2.save('pict-1920x1080.png')

***End-of-Code***
```

Appendix C: Python Code for Data Capture

```
***Begin-Code***

import nidaqmx

import numpy as np

import matplotlib.pyplot as plt

from nidaqmx.constants import AcquisitionType, Edge

Samples_Per_Sec = 500000

Samples_Per_Ch_To_Read = 500000*60

data = np.zeros((1,Samples_Per_Ch_To_Read), dtype=np.float64)

with nidaqmx.Task() as task:

    task.ai_channels.add_ai_voltage_chan("Dev2/ai0")

    task.timing.cfg_samp_clk_timing(Samples_Per_Sec, source="",

active_edge=Edge.RISING, sample_mode=AcquisitionType.FINITE,

samps_per_chan=Samples_Per_Ch_To_Read)

    data =

task.read(Samples_Per_Ch_To_Read,timeout=nidaqmx.constants.WAIT_INFINITELY)

    print(len(data), " data points in array")

    print("Samples_Per_Sec = ", Samples_Per_Sec)

    print("Samples_Per_Ch_To_Read = ",Samples_Per_Ch_To_Read)

    #np.savetxt("710nm-Airy00-ZERO-50mW-0p000mlps-1200hz-PMT250-FloatingPotential-

1sec.csv",data, delimiter=",")

    np.savetxt("PMT300-1200hz-000mWGauss-DARK-TableGrounded-BlueIceCold-

60sec.csv",data, delimiter=",")

    #print(data)

    time = (Samples_Per_Ch_To_Read / Samples_Per_Sec)

    st_time = str(time)
```

```
#Sample_Cnt = np.arange(0,Samples_Per_Ch_To_Read,1)

#plt.plot (Sample_Cnt,data, "bo-", label='PMT v', linewidth=0.5)
#plt.xlabel("samples read")
#plt.ylabel("voltage (V)")
#plt.legend()
#plt.axis ([-1,Samples_Per_Ch_To_Read, -1,10])
#plt.show

print("Time in Seconds: ", time)
print (np.mean(data))

***End-of-Code***
```

Vita

Aurelio Paez is a single father of 4 children. Raised in southern California then brought to the American Southwest by his parents, he had shown an affinity to mathematics, computers, science, and disassembly of electronics.

Aurelio Paez attended The University of Texas at El Paso where he received his Bachelor of Science in Physics in 2012. As an undergraduate he did research in astrophysics, collecting and analyzing data on black hole candidate SWIFT J1753.4-0126. He won the COURI award in bioinformatics and modeling for his work. He worked as a T.A. through out his academic career and won the departments “Best T.A.” award on two separate occasions.

He continued at UTEP and received his Master of Science in Physics in 2014. He studied titanium doped tungsten oxide thin films and co-authored a paper on boron doped diamonds.

In 2019 he graduated with a Doctorate in Materials Science and Engineering from The University of Texas at El Paso. During this time, he was able to write a primary author paper on Non-linear optical flow cytometry, in addition to co-authoring 4 articles. His studies included nano-particle uptake tracing in sweet potato, tissue engineering of a novel photo-cleavable material, and the application of non-linear optics to flow cytometry. In addition to his coursework and research, he also spent 2 semesters working at NASA’s Marshall Space Flight Center, where he worked on the space environments team. This co-op led to a job offer as an Aerospace Engineer directly out of the PhD.

Contact Information: aurelio.paez@gmail.com